CANCER

A synergistic interaction between PRMT5 and LSD1 inhibitors in AML

Nesteene Joy Param[1]†, Elisa Arceci[1]†, Francesco Fiorentino[2,3]†, Luca Pignata[4,5]†, Denis Torre[1]†, Nayeli Gutiérrez-Trejo[1], Jia Yi Fong[4,5], Pierre-Alexis Goy[4,5], Brenda Y. Han[4,5], Chiara Lambona[2], Elisabetta Di Bello[2], Carola Castiello[2], Marco Barone[6]‡, Megan Schwarz[1], Cheryl Arrowsmith[7], Koichi Ito[8], Peggy Scherle[8], Dave Keng Boon Wee[4], Steven Ndoye[1], Tommaso Tabaglio[4,5], Anand D. Jeyasekharan[9,10], Manikandan Lakshmanan[4], Roberto Cirilli[11], Hansjörg Habisch[12,13], Tobias Madl[12,13], Andrea Mattevi[6], Sergio Valente[2]*, Antonello Mai[2]*, Ernesto Guccione[1]*

Acute myeloid leukemia (AML) is a hematopoietic malignancy caused by abnormal proliferation and differentiation of blasts. PRMT5, a methyltransferase that catalyzes symmetric dimethylation of arginine (SDMA) residues, has been implicated in cancer stem cell homeostasis and shown to be a potential therapeutic target in AML. However, given the toxicity of complete PRMT5 inhibition, there is a need to identify effective synergistic therapies. Through a targeted screen of compounds that inhibit key nodes of PRMT5-regulated pathways, we identified a synthetic lethality between inhibition of PRMT5 and LSD1, a lysine demethylase known to affect AML blast differentiation. The two inhibitors broadly reshape the transcriptome of targeted cells and synergize to promote AML differentiation and eventually growth inhibition and apoptosis, in a p53-dependent manner. To leverage this synthetic lethal interaction, we generated new dual compounds to inhibit both enzymes and recapitulated the effects of the drug combination. Our results uncover an unexpected convergence of PRMT5- and LSD1-regulated targets, paving the way for new therapeutic opportunities.

INTRODUCTION

Acute myeloid leukemia (AML) is a heterogeneous family of diseases (*1*) with oncogenic drivers belonging to distinct functional classes such as signaling (e.g., FLT3 and PTPN1), cell differentiation (e.g., CEBPα and RUNX1), cell cycle/apoptosis (e.g., NPM1 and TP53), epigenetic modifiers (e.g., TET2 and IDH1/2), and splicing (e.g., SF3B1, SRSF2, U2AF1, and ZRSR2), being affected by transcriptional deregulation, point mutations, or chromosomal rearrangements (*2*–*4*). These leukemias are characterized by abnormal differentiation and proliferation of a clonal population of myeloid stem cells, called blasts. Blasts are unable to terminally differentiate, and as a result, their number increases aberrantly (*5*, *6*). Genome-wide screens targeting chromatin and transcriptional cofactors have identified vulnerabilities that can be potentially exploited for therapeutic purposes, including targeting of the two major arginine methyltransferases PRMT1 and PRMT5 (*7*).

PRMTs are arginine methyltransferases catalyzing the transfer of methyl group(s) from *S*-adenosyl-L-methionine (SAM) to the protein substrate arginine side chain, and they can be divided into three subgroups: type I (PRMT1, 2,3, 4, 6, and 8), type II (PRMT5 and 9), and type III (PRMT7). All three subtypes are able to catalyze monomethylation of arginine (MMA), but only type I PRMTs are able to catalyze asymmetric dimethylation of arginine (ADMA), whereas type II PRMTs catalyze symmetric dimethylation of arginine (SDMA) (*8*).

We and others have demonstrated that inhibition of PRMT5 or type I PRMTs has been linked to several downstream effects and proven to affect multiple oncogenic pathways (*9*). In the past few years, several synthetic lethal interactions with PRMT1/5 inhibitions have been described. First, we described that MYC-driven lymphomas are particularly susceptible to PRMT5 inhibition, due to a key dependency on a highly active splicing machinery (*10*, *11*). Next, seminal papers have documented that tumors with an MTAP deletion are more susceptible to further depletion of PRMT5 (*12*–*14*) or inhibition of type I PRMTs (*15*, *16*). Last, we reported that AML driven by splicing factor mutations (i.e., SRSF2, SF3B1, and U2AF1) are sensitive to both PRMT1 and PRMT5 inhibition (*17*).

Here, we aimed to identify additional synthetic lethal interactions, and to do so, we set up a screen to uncover vulnerabilities of AML cells with a reduced PRMT5 activity. Inhibition of LSD1, an enzyme that catalyzes the demethylation of mono- and dimethyl lysine residues (e.g., H3K4me1/2 and H3K9me1/2) (*18*–*24*), synergized with PRMT5 inhibition in multiple AML models both in vitro and in vivo. The two inhibitors broadly reshape the transcriptome of targeted cells and synergize to promote AML differentiation and eventually growth inhibition and apoptosis, in a p53-dependent manner. To leverage this interaction, we lastly generated a new set of dual compounds that simultaneously inhibit both enzymes.

[1]Center for OncoGenomics and Innovative Therapeutics (COGIT); Center for Therapeutics Discovery, Department of Oncological Sciences and Pharmacological Sciences, Tisch Cancer Institute, Icahn School of Medicine at Mount Sinai, NY, New York, USA. [2]Department of Drug Chemistry and Technologies, Sapienza University of Rome, 00185 Rome, Italy. [3]Department of Biochemical Sciences, Sapienza University of Rome, 00185 Rome, Italy. [4]Institute of Molecular and Cell Biology, Agency for Science, Technology and Research (A*STAR), Singapore 138673, Singapore. [5]Department of Biochemistry, Yong Loo Lin School of Medicine, National University of Singapore, Singapore 119077, Singapore. [6]Department of Biology and Biotechnology, University of Pavia, 27100 Pavia, Italy. [7]SGC Toronto, Toronto, Canada. [8]Prelude Therapeutics, Wilmington, DE, USA. [9]Cancer Science Institute of Singapore, National University of Singapore, Singapore, Singapore. [10]Department of Haematology-Oncology, National University Hospital, Singapore, Singapore. [11]Centre for the Control and Evaluation of Medicines, Chemical Medicines Unit, Istituto Superiore di Sanità, Viale Regina Elena 299, 00161 Rome, Italy. [12]Gottfried Schatz Research Center for Cell Signaling, Metabolism and Aging, Molecular Biology and Biochemistry, Medical University of Graz, Graz, Austria. [13]BioTechMed-Graz, Graz, Austria.
*Corresponding author. Email: sergio.valente@uniroma1.it (S.V.); antonello.mai@uniroma1.it (A. Mai); ernesto.guccione@mssm.edu (E.G.)
†These authors contributed equally to this work.
‡Present address: Center for the Advanced Study of Drug Action and Department of Chemistry, Stony Brook University, Stony Brook, NY 11794-3400, USA.

Mechanistically, these dual compounds elicit transcriptional and posttranscriptional (splicing) defects that recapitulate the combination therapy. The x-ray cocrystal structure of one of the designed inhibitors with LSD1 was identified, elucidating its binding mode and providing a structural basis for the rational design of further inhibitors.

RESULTS

A chemical screen identifies synthetic lethal interactions with PRMT5

To identify synthetic lethal interactions with PRMT5, we set up a targeted small molecule screen, using compounds that inhibited key nodes of known PRMT5-regulated pathways (table S1). According to the "threshold model" of PRMT5 activity, based on which normal cells can still function with up to 15 to 20% residual PRMT5 activity, although cancer cells require >50% activity (*9*), we generated isogenic MLL-AF9–driven murine AML cells, either wild-type ($Prmt5^{+/+}$) or heterozygous ($Prmt5^{+/-}$) for PRMT5 (fig. S1A). The hypothesis was that drugs that would dampen PRMT5 activity, and/or perturb similar pathways to PRMT5, would selectively kill $Prmt5^{+/-}$ MLL-AF9 over $Prmt5^{+/+}$ MLL-AF9.

We tested five different concentrations for each drug based on recommended median inhibitory concentration (IC_{50}) values (*25*) in MLL-AF9 $Prmt5^{+/+}$ and MLL-AF9 $Prmt5^{+/-}$ AML cells for 7 days. After treatment, we assessed cell viability using an MTS assay (Fig. 1A and fig. S1B), and we observed that, whereas some drugs reduced viability in both $Prmt5^{+/-}$ MLL-AF9 and $Prmt5^{+/+}$ MLL-AF9, others preferentially targeted $Prmt5^{+/-}$ cells. Among the drugs that more selectively killed $Prmt5^{+/-}$ cells, we identified known synergistic drugs [e.g., MS023 (a type I PRMT inhibitor) and E7107 (an SF3B1 inhibitor)] (*17*), chemotherapeutic drugs (e.g., cisplatin) (*26*, *27*), as well as novel candidates (e.g., drugs targeting chromatin modifiers such as LSD1 and Topoisomerase1 or kinases such as CK2, CDK4/6, and ERK1/2) (Fig. 1A and tables S1 to S5). This first screen has identified promising candidates for combinatorial therapy in AML, using PRMT5 inhibition as an anchor.

PRMT5 and LSD1 inhibition synergize to reduce tumor growth in vitro and in vivo

To test these promising targets, we performed a counter screen combining shortlisted molecules with a SAM-competitive PRMT5 inhibitor, PRT220 (Prelude Therapeutics, chemical structure not disclosed). We incubated MV4-11 cells with different concentrations of drugs alone, or in combination, for 6 days and then measured cell viability using CellTiter-Glo assay. All values were normalized to dimethyl sulfoxide (DMSO) control, and drug interactions were evaluated using five different synergy models: (i) Chou-Talalay combination index (CI), (ii) Bliss, (iii) Highest Single Agent (HSA), (iv) Loewe, and (v) Zero Interaction Potency (ZIP) (*28*, *29*). Across all dose-response matrices generated from three different AML cell lines (MV4-11, K562, and U937), every model consistently identified synergistic interactions between PRT220 and GSK-LSD1 (Fig. 1, B to D; fig. S1, B to D; and tables S3 and S4). In contrast, other drug combinations produced inconsistent results across synergy models, which guided our decision to pursue PRMT5 inhibition combined with LSD1 inhibition (fig. S1C and table S5).

LSD1 is an enzyme catalyzing the removal of mono- and dimethyl marks of lysine residues from both histone (i.e., H3K4me1/2 and H3K9me1/2) and nonhistone proteins (*18*–*24*, *30*). To confirm drug-target engagement, we performed Western blot analysis using MV4-11–treated cells for 3 days. To validate the efficacy of LSD1i, we checked levels of H3K4me1 and H3K4me2, whereas for PRMT5i, we checked the level of SDMA, as well as ADMA and MMA as controls. As expected, we observed a reduction of SDMA in cells treated with PRMT5i and an increase in H3K4me1 and H3K4me2 in cells treated with LSD1i (fig. S1D).

Next, we confirmed the effectiveness of the drug combination in vivo. Briefly, 5 million MV4-11 cells were injected subcutaneously in the flank of a small cohort of mice and the treatment was started at 10 days postinjection when the tumors were palpable. We treated mice with PRMT5i (10 mg/kg, oral gavage), LSD1i (0.15 mg/kg, intraperitoneally), or combination of both drugs. The combination treatment decreased tumor volume by 68%, whereas PRMT5i and LSD1i monotherapy reduced tumor volume by only 31 and 45%, respectively (fig. S1E). Moreover, we did not observe differences in body weight during treatment, suggesting that the treatment is not toxic and well tolerated (fig. S1F).

PRMT5 and LSD1 inhibition converge to transcriptionally regulate pathways linked to cell differentiation

To understand the mechanism underlying the synergistic cytotoxic effects of combinatorial PRMT5 and LSD1 inhibition, we performed RNA sequencing (RNA-seq) on MV4-11 cells treated with DMSO, PRMT5i (3 nM), LSD1i (10 nM), or both drugs (P5i + Li) combined for 3 days. We chose a relatively early time point to capture primary, rather than secondary, effects. Analysis of gene expression was performed to determine whether there were changes in expression patterns that could explain the synergistic phenotype seen upon PRMT5i and LSD1i combination in MV4-11. The first relevant observation is that both drugs converge on the transcriptional regulation of common targets (exemplified by a positive correlation of $R = 0.29$ of the perturbed transcriptome and an overlap of 61 up-regulated and 23 down-regulated genes) (Fig. 2, A and B), potentially explaining synergy. Although correlation analysis confirmed that the combination recapitulates single treatments with LSD1i and PRMT5i alone ($R = 0.88$ and $R = 0.57$, respectively) (Fig. 2A), we observed a greater degree of deregulated genes in the combination treatment (Fig. 2B and table S6). As expected, LSD1i caused an increase in genes associated with antigen processing and presentation (e.g., *HLA-DR*, *CCL2*, and *CXCR3*), which are associated with myeloid differentiation (fig. S2A and tables S6 and S7). PRMT5 inhibition (fig. S2B and tables S6 and S7), and more so the combined LSD1/PRMT5 inhibition (Fig. 2C and tables S6 and S7), led to deregulation of a similar gene set. Flow cytometry analysis validated these findings with increased levels of CD11b and CD86 as well as increased levels of other differentiation markers, like CD45RA, CD68, CD80, HLA-DR, CD163, and CD206 in the combination compared to single treatments (Fig. 2D and fig. S2C). As for genes that were down-regulated upon drug treatment, we observed a down-regulation of genes associated with cell division (e.g., "mitotic sister chromatid segregation") in P5i + Li–treated cells, suggesting decreased replication in combination treatment (Fig. 2C and tables S6 and S7). To summarize, both flow cytometry and RNA-seq demonstrate reduced proliferation and increased differentiation in PRMT5- and LSD1-inhibited AML cells, with a synergistic effect when both drugs are combined.

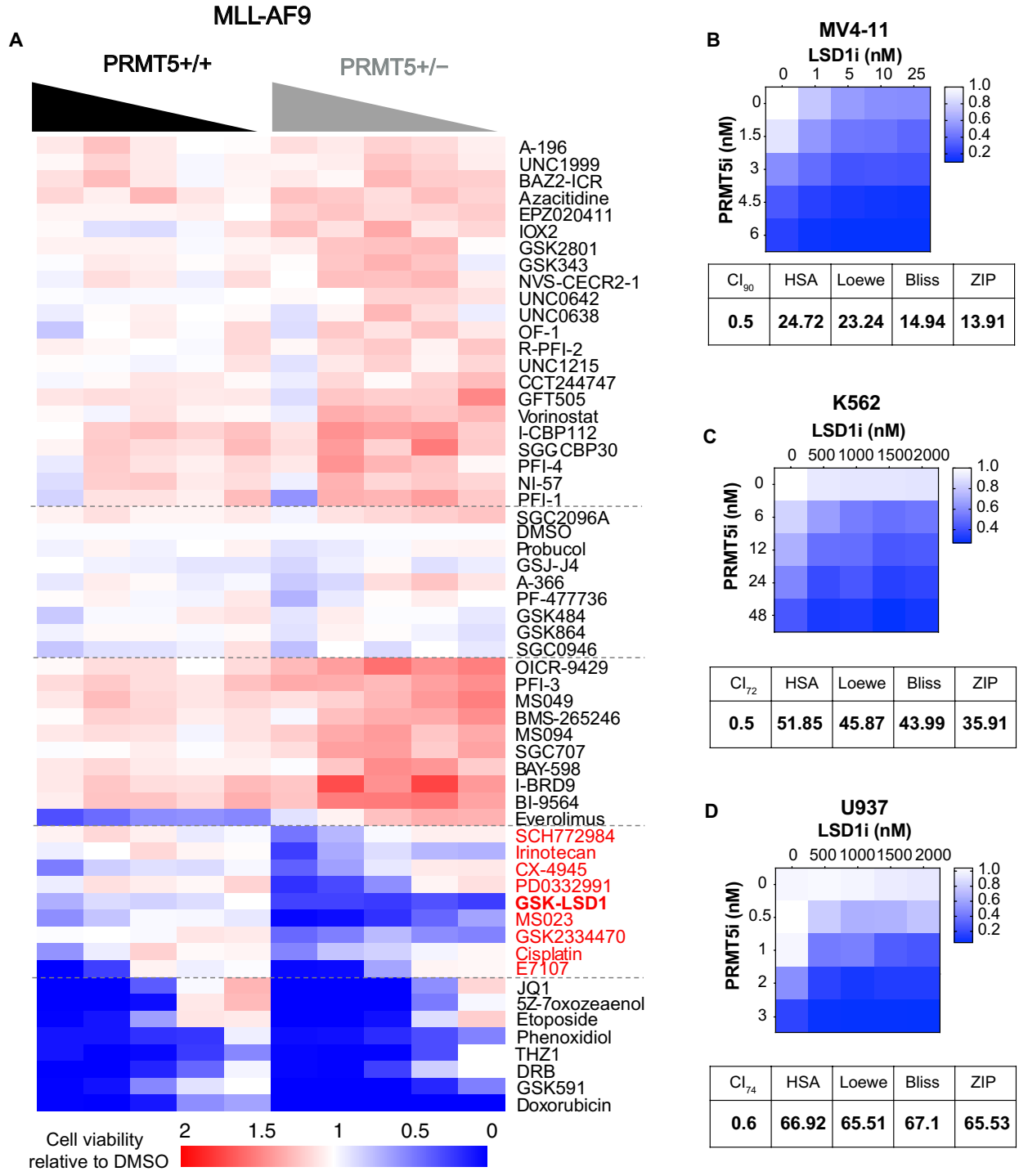

CI_{90}	HSA	Loewe	Bliss	ZIP
0.5	**24.72**	**23.24**	**14.94**	**13.91**

CI_{72}	HSA	Loewe	Bliss	ZIP
0.5	**51.85**	**45.87**	**43.99**	**35.91**

CI_{74}	HSA	Loewe	Bliss	ZIP
0.6	**66.92**	**65.51**	**67.1**	**65.53**

Fig. 1. A chemical screen identifies synthetic lethal interactions with PRMT5 inhibition. (**A**) MLL-AF9 Prmt5$^{+/+}$ and MLL-AF9 Prmt5$^{+/-}$ cells were treated for 7 days with commercially available inhibitors (five concentrations per compound). Viability was assessed via the MTS assay, normalized to DMSO, and reported as ratio over DMSO (blue indicates lower cell viability compared to DMSO, and red indicates higher cell viability compared to DMSO). The name of drugs preferentially killing MLL-AF9 Prmt5$^{+/-}$ is highlighted in red. (**B** to **D**) Viability heatmaps of (B) MV4-11, (C) K562, and (D) U937 cells treated for 6 days with PRT220 (PRMT5i) in combination with GSK-LSD1 (LSD1i) and synergy scores quantified using CI (CI < 1: synergism; CI = 1: additive; CI > 1: antagonism), HSA (score > 0: synergy; score = 0: additive; score < 0: antagonism), Loewe, Bliss, and ZIP (score > 10: synergy; −10 to 10: additive; score < −10: antagonism). Cell viability as assessed via CellTiter-Glo and normalized to DMSO control.

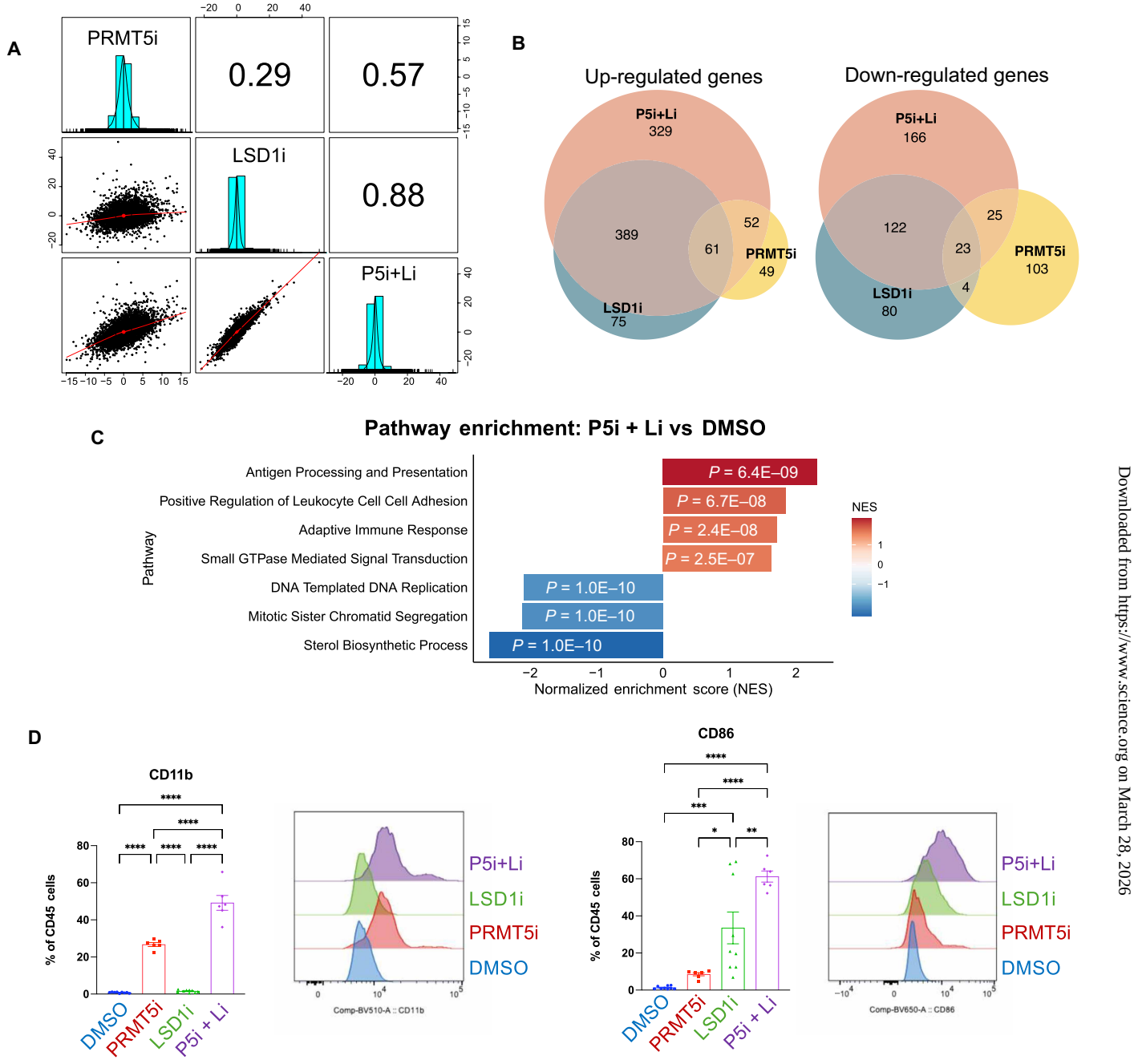

Fig. 2. PRMT5 and LSD1 inhibition synergize to induce myeloid cell differentiation. (**A**) Correlational graphs of up-regulated and down-regulated genes between PRMT5i, LSD1i, and P5i + Li in MV4-11–treated cells for 3 days. (**B**) Venn diagram of the differential gene overlap between PRMT5i, LSD1i, and P5i + Li in MV4-11 3 days posttreatment. (**C**) GSEA of MV4-11 cells treated with P5i + Li compared to DMSO. (**D**) Percentage of CD11b- and CD86-expressing cells in CD45-positive cells in DMSO-, PRTM5i-, LSD1i-, and P5i + Li–treated MV4-11 at day 6 with representative histograms. Statistical analysis performed with two-way analysis of variance (ANOVA). Error bars represent SEM. *$P \leq 0.05$; **$P \leq 0.01$; ***$P \leq 0.001$; ****$P \leq 0.0001$.

PRMT5 and LSD1 inhibition synergize to induce apoptosis in a p53-dependent manner

We and others have reported that the cytoplasmic PRMT5-MEP50-pICln complex methylates several ribose-binding proteins (RBPs) (*31*) including Sm proteins, which are critical for the correct maturation of small nuclear ribonucleoproteins (snRNPs), the main components of the spliceosome (*10*, *32*–*35*). Therefore, PRMT5 inhibition is known to reduce splicing fidelity, resulting in altered splicing patterns of important genes involved in proliferation and DNA damage response (DDR), such as *MDM4* (*36*), *ATR* (*10*), and *TIP60* (*37*). To assess the impact on splicing of the PRMT5 and LSD1 inhibitors in MV4-11, we performed splicing analysis [rMATS (*38*)]. Although,

as expected, PRMT5 inhibition led to well-described increase in intron retention and deregulation of exon skipping events, LSD1i induced less pronounced effects (Fig. 3, A and B). Nonetheless, both single drug or combination treatment led to deregulation of overlapping events in genes involved in cell cycle and cellular response to stress (fig. S3, A to C, and table S8).

A recent study reported that AML cells are more sensitive to LSD1 inhibition when P53 is expressed, and small molecules targeting LSD1 are stabilizing P53 and increasing its transcriptional activity (*39*, *40*). Given that PRMT5i is known to activate the p53 pathway (*36*), we wanted to test whether the synergistic effect of the two drugs was linked to P53 activation.

The hypothesis was that inhibition of PRMT5 may decrease the level of MDM4 protein [negative regulator of P53 function (*36*)], by inducing the skipping of *MDM4 exon 6*, and this would, in turn, lead to an increased TP53 activity, sensitizing cells to LSD1 inhibition. PRMT5i treatment induces *MDM4 exon 6* skipping (Fig. 3C), leading to a decrease in MDM4 protein after 3 days of treatment (Fig. 3D and fig. S3, D and E). Combination treatment leads to an increase in splicing compared to PRMT5i alone, corresponding to further induction of P53 levels (Fig. 3, C and D). Overall, both single and combined inhibition of PRMT5 and LSD1 converge on the activation of the TP53-regulated DDR (Fig. 3E).

To demonstrate that the presence of P53 played a role in the sensitivity to the P5i + Li, we next created isogenic MV4-11 lines by knocking out *TP53* ($P53^{WT}$ and $P53^{KO}$, respectively). Upon treatment of $P53^{WT}$ and $P53^{KO}$ cells with DMSO, PRMT5i, and/or LSD1i for 6 days, we observed a decrease in synergistic effects of P5i + Li in viability (Fig. 3F) with decreased apoptotic capacity (Fig. 3G) in $P53^{KO}$ cells. These data provide a direct mechanistic link between the presence of wild-type P53 and the effect of the simultaneous inhibition of PRMT5 and LSD1.

Development of first-in-class dual-targeting LSD1/PRMT5 inhibitors

The pronounced synergy observed with the simultaneous inhibition of PRMT5 and LSD1 inspired the development of first-in-class dual-targeting hybrid inhibitors designed to target both enzymes simultaneously. Such dual inhibitors could offer considerable pharmaceutical advantages over single-target inhibitors. They have the potential to provide enhanced efficacy in terms of cellular viability and target engagement, surpassing what can be achieved with individual PRMT5 or LSD1 inhibitors. In addition, administering a single compound rather than a combination of two drugs would simplify the clinical translation, reducing regulatory and logistical challenges.

With this rationale in mind and our extensive experience in the design and synthesis of tranylcypromine (TCP)–based LSD1 inhibitors (*41*–*49*), we initiated the design and synthesis of novel dual LSD1/PRMT5 inhibitors. These new molecules were designed by integrating structural elements of the LSD1i and the PRMT5 inhibitor, GSK591, whose chemical structure is well known (Fig. 4).

Biochemical evaluation toward LSD1 and PRMT enzymes

Following their synthesis and characterization (see the Supplementary Materials), all the final compounds were tested in enzymatic assays to evaluate their inhibition activity against LSD1 and PRMT5 and against PRMT1 and PRMT7 to assess their specificity for PRMT5 over other methyltransferases. The LSD1 inhibition assay was conducted by using the LSD1/CoREST complex and the dimethyl lysine 4 histone H3 (residues 1 to 21) peptide (H3K4me2) as the substrate. The compound used as the positive control was TCP. The assays toward PRMTs were conducted by using the human PRMT5/MEP50 complex, human PRMT1, and human PRMT7 with histone H2A, histone H4, and GST-GAR as substrates, respectively. The compound used as reference was *S*-(5′-adenosyl)-L-homocysteine (SAH).

By analyzing the results obtained by the LSD1 inhibition assays, all the new hybrid compounds were more potent than TCP (Fig. 5). To ascertain that the PRMT5i GSK591 was not endowed with any LSD1 inhibition activity, we tested it against this target and observed no inhibition even at the highest concentration (500 μM) (fig. S4, A and B). GSK591 inhibition of PRMT targets has been well characterized (*50*). GSK591 is selective for PRMT5 compared to a panel of other methyltransferases including PRMT1 and PRMT7 (*50*). With respect to the stereochemistry of the compounds, we found that, among the derivatives lacking a spacer between the two enzyme-targeting moieties (**1a** and **1b**), the (*R*)-diastereoisomer (referred to the carbinolic carbon) **1b** was about twice as potent as the (*S*)-diastereoisomer **1a**. The same trend was found for derivatives bearing methylene spacer, with the (*R*)-diastereoisomer **2b** being about twice as potent as its (*S*)-counterpart **2a** (fig. S4, C and D). This was unexpected because GSK591 has its chiral center at the carbinol bridge with the (*S*) configuration; therefore, LSD1 preferentially interact with the carbinol moiety in opposite stereochemistry respect to PRMT5. Moreover, the insertion of the methylene spacer is detrimental for the inhibition potency because both compounds **2a,b** were 40-fold less potent when compared to the corresponding shorter derivatives (**1a** and **1b**) (fig. S4, E and F). Last, for the two derivatives with the cycloalkylamine spacer, both synthesized as (*S*)-diastereoisomers at the carbinolic center according to the configuration of GSK591, the inhibitory activity of compound **4** containing the piperidine moiety was about twofold stronger than compound **3** containing the azetidine portion. Overall, these compounds, containing a longer linker, are only slightly less potent than the short derivatives **1a,b** but they turn out to be more potent than the derivatives with the methylene spacer **2a,b** (Fig. 5 and fig. S4, G and H).

Regarding the inhibitory activity against PRMT5, all compounds show a potent inhibition in the nanomolar range with a good selectivity over the PRMT1 and PRMT7 isoforms (Fig. 5). In particular, the best compounds **1a** and **4** displayed IC_{50} values of 14 and 43 nM, respectively. We chose these two compounds for further biological analysis and will be referred to as MC4455 (**1a**) and MC4491 (**4**). The biochemical data show that our strategy to design LSD1/PRMT5 dual hybrid inhibitors was successful, considering that all compounds have good inhibition properties against both targets being selective over other PRMT members (Fig. 5).

MC4455 was also assessed in a thermal shift assay, showing that it could stabilize the LSD1/CoREST complex as it increased the protein unfolding temperature by 8.4°C. Moreover, we demonstrated that MC4455 binds covalently to the flavin adenine dinucleotide (FAD) cofactor of LSD1, as proven by the rapid bleaching of the oxidized flavin absorbance peak at 458 nm after a few minutes of incubation with the inhibitor (Fig. 6A).

Structural analysis of MC4455 binding to LSD1 and PRMT5

Next, we solved the crystal structure of the LSD1/CoREST-MC4455 complex, which indicated that the inhibitor has the binding pose

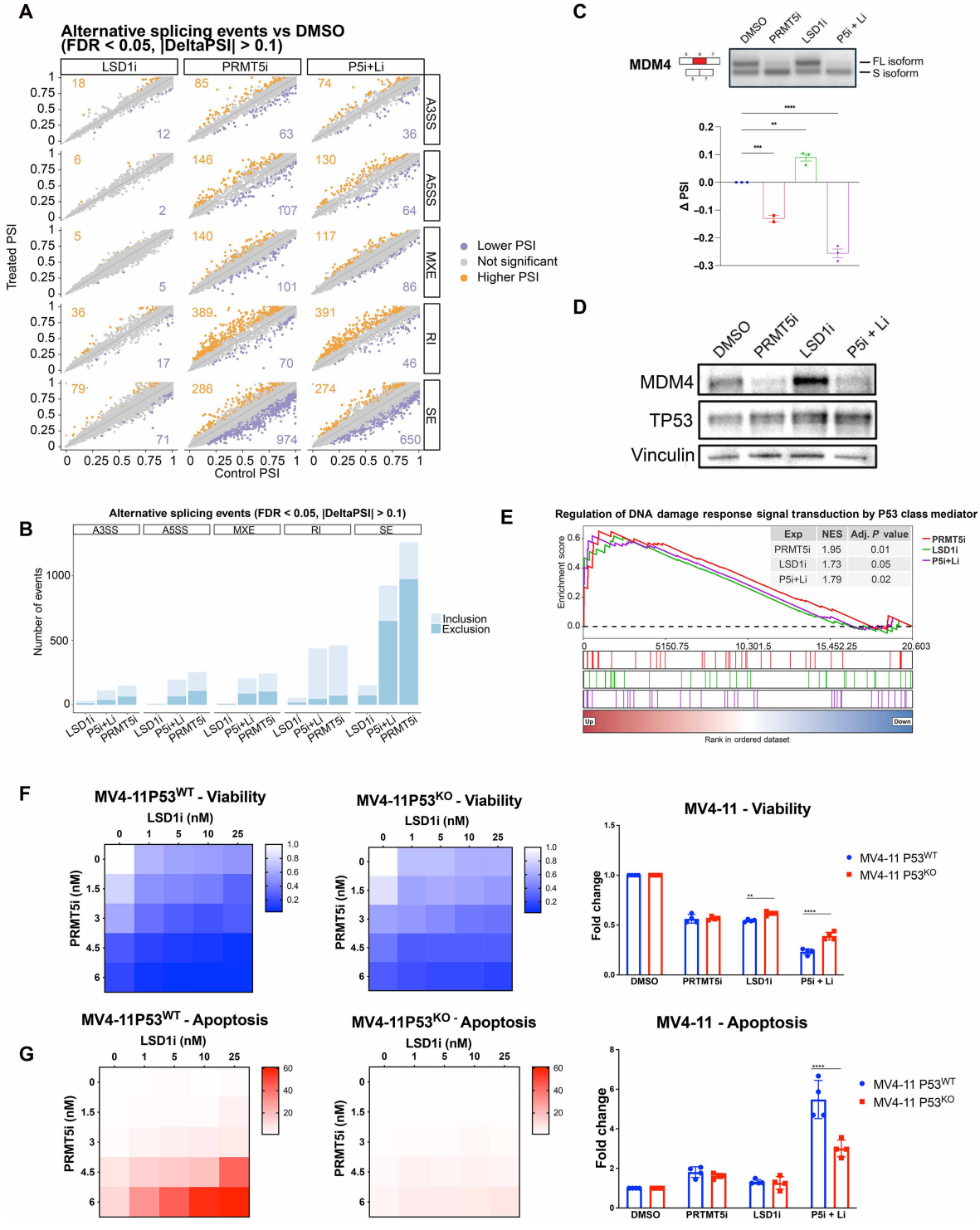

Fig. 3. PRMT5 and LSD1 inhibition synergize to induce cell differentiation and apoptosis in a p53-dependent manner. (**A**) Differentially expressed alternative splicing events in MV4-11 cells treated for 3 days with LSD1i, PRMT5i, and P5i + Li treatment: alternative 3′ splice site (A3SS), alternative 5′ splice sites (A5SS), mutually exclusive exon (MXE), intron retention (RI), and exon skipping (SE) with inclusion and exclusion. ΔPSI levels of each treatment is compared to DMSO. ΔPSI of splicing events > 0.1 is considered significant. (**B**) Alternative splicing events in MV4-11 cells treated with LSD1i, PRMT5i, and P5i + Li for 3 days. (**C**) Reverse transcription PCR (RT-PCR) of *MDM4 exon 6* in MV4-11 cells treated for 3 days. ΔPSI levels quantified from RT-PCR normalized to DMSO. (**D**) Western blot of MDM4 and P53 in MV4-11 treated for 3 days. (**E**) Normalized enrichment score (NES) for the pathway "Regulation of DNA Damage Response Signal Transduction by P53 Class Mediator" for PRMT5i, LSDi, and P5i + Li. (**F**) Cell viability matrix of MV4-11P53^{WT} and MV4-11P53^{KO}. Cells were treated with PRMT5i, LSD1i, or P5i + Li for 6 days, and cell viability was determined by CellTiter-Glo. (**G**) Caspase activation matrix of MV4-11P53^{WT} and MV4-11P53^{KO} cells treated with PRMT5i and LSD1i and the fold change of caspase activation of cells treated with PRMT5i, LSD1i, or P5i + Li performed using Caspase-Glo 3/7. Statistical analysis performed with one-way ANOVA. Error bars represent SEM. *$P \leq 0.05$; **$P \leq 0.01$; ***$P \leq 0.001$; ****$P \leq 0.0001$.

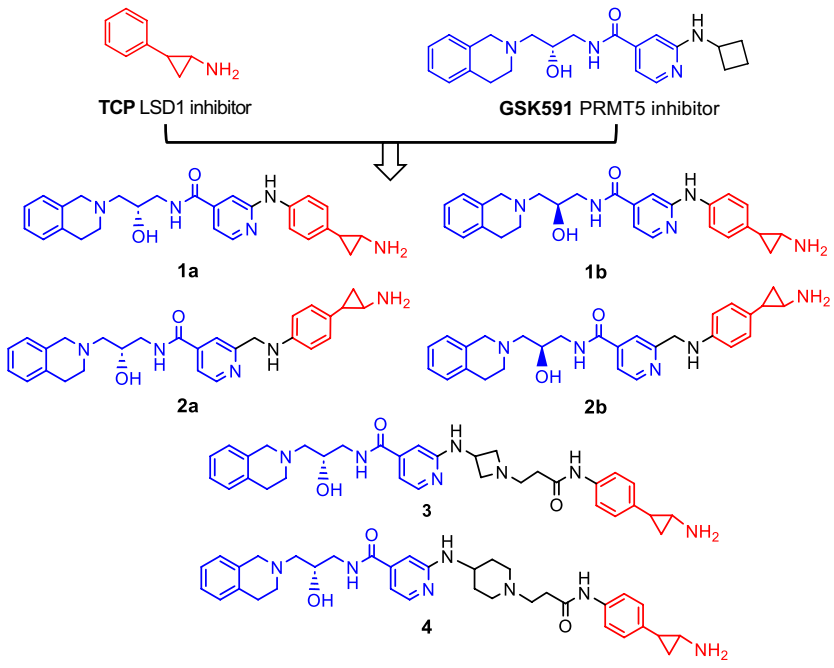

Fig. 4. Design of the first-in-class dual hybrid LSD1/PRMT5 inhibitors. Inhibitors derived from compounds that were structurally known, such as TCP for LSD1 inhibition and GSK591 for PRMT5 inhibition. Six compounds were produced: compounds **1a**, **1b**, **2a**, **2b**, **3**, and **4**. **1a** and **1b** are derivatives with no spacers between the two enzymes' warheads. **2a** and **2b** are derivatives with methylene spacers. **3** and **4** are derivatives with an azetidine moiety and a piperidine moiety, between the two enzymes' warheads.

classically found for the anti-LSD1 compounds based on the TCP scaffold. This includes the presence of a covalent bond with the N5 atom of the flavin moiety of FAD (*51*) (Fig. 6, B to E). The elongated MC4455 molecule protrudes toward the rim of the LSD1 catalytic cleft, interacting with several residues that stabilize the molecule in a well-defined conformation as clearly defined by the electron density map. Analysis of the three-dimensional structure shows several hydrophobic contacts with V333, L386, F538, W552, and A809, an electrostatic interaction between D556 and the nitrogen of the tetrahydroisoquinoline moiety of MC4455, and π-stacking (t-shape) between W552 and the benzene ring of the tetrahydroisoquinoline (Fig. 6E).

We also performed docking experiments to capture the interactions between MC4455 and PRMT5. To this end, we used the cocrystal structure of the PRMT5/MEP50 complex bound to GSK591 and sinefungin [Protein Data Bank (PDB) ID: 5C9Z] as the starting model for the simulations. We initially benchmarked the docking parameters for their ability to reproduce the binding conformation of GSK591 in the pocket. The resulting pose closely matched the crystallographic binding mode (fig. S5A), recapitulating the same network of hydrogen bonds and hydrophobic contacts observed in the cocrystal structure. We then modeled the binding mode of MC4455 to PRMT5 and compared it with that of GSK591. MC4455 was predicted to bind in the same pocket, adopting a similar orientation to GSK591. The region corresponding to the GSK591 moiety aligned closely with the reference pose, whereas the TCP group remained solvent exposed (fig. S5, B and C). The interaction profile was largely conserved, with hydrogen bonds with the backbone carbonyl of L437 and the backbone amides of F577 and F580 retained in the docked prediction. In addition, docking predicted new hydrogen bonds: one between the hydroxyl group of MC4455 and the indole nitrogen of W579 and another between the carbonyl group of MC4455 and the side-chain hydroxyl of S439 (fig. S5, B and C). Last, to assess target engagement, we quantified the activity of the dual compound MC4455 in MV4-11 cells. As expected, MC4455 reduces SDMA levels similarly to GSK591 (591) and increases H3K4me2 levels like GSK-LSD1 (Li) (fig. S5, D to F).

The dual LSD1/PRMT5 inhibitor recapitulates the effect of drug combination

Last, we decided to assess whether compound MC4455 and MC4491 would recapitulate the effects on transcription and splicing, observed upon PRMT5i and LSD1i treatment. MV4-11 cells were treated with 50 nM MC4455 and MC4491 for 3 days and RNA extracted and sequenced.

As expected, we observed a high correlation between the transcriptomic changes (Fig. 7A), the deregulated pathways (Fig. 7B, fig. S6A, and table S9), and the splicing alternations (Fig. 7, C and D; fig. S6, B and C; and table S10). If we plot our samples based on the log fold change in transcript abundance (x axis) and splicing perturbation (y axis) (see Materials and Methods), compared to DMSO (Fig. 7E), it is clear that PRMT5 inhibition mainly affects splicing, whereas LSD1 inhibition mainly contributes to changes in transcript abundance, yet they converge on regulating similar pathways (Figs. 2 and 3 and figs. S2 and S3), explaining the synergistic interaction.

Further biological testing was done only on MC4455 because both inhibitors recapitulated the combination treatment. To test differentiation activity, we used GSK591 as the single-agent control and in combination with GSK-LSD1 (591 + Li) because MC4455 was modeled on these scaffolds.

Cpds	Molecular structure	IC_{50} (μM) or % inhibition at 100 μM			
		LSD1/ CoREST	PRMT1	PRMT5/ MEP50	PRMT7
1a (MC4455)	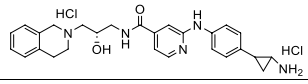	0.104	NI*	0.014	10.4%
1b	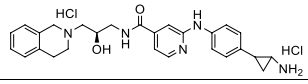	0.044	6.2%	0.016	43.2%
2a	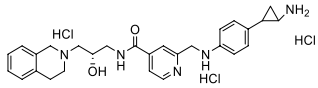	3.70	NI	0.12	31%
2b	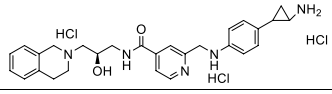	1.74	4.5%	1.99	7.7%
3	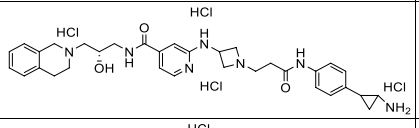	0.263	46.6%	0.059	42.8
4 (MC4491)	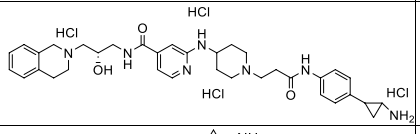	0.152	3.5%	0.043	11.7%
TCP	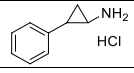	40.8	NT†	NT	NT
SAH	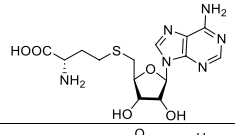	NT	0.247	1.41	0.290
GSK591	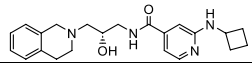	NI (at 500 μM)	NI (*50*)‡	0.004 (*50*)	NI (*50*)

*NI, no inhibition at 100 μM. †NT, not tested. ‡Not tested in this manuscript, but tested in (*50*).

Fig. 5. IC_{50} values for dual LSD1/PRMT5 hybrid inhibitors (1a, 1b, 2a, 2b, 3, and 4) and reference compounds (TCP, SAH, and GSK591) against LSD1/CoREST, PRMT1, PRMT5/MEP50, and PRMT7.

Using the IC_{50} of MC4455 in MV4-11 cells after a 6-day treatment, MC4455 increased CD11b-positive cells compared to combination and all single-agent treatments while exhibiting similar or lower levels of expression for other differentiation marks (Fig. 7F and fig. S6D). These results suggest that the relative potency and mechanism of inhibition of PRMT5 and LSD1 through MC4455, compared to PRT220, GSK591, and GSK-LSD1, induce activation of specific differentiation makers, which deserves further future investigation.

DISCUSSION

The lysine-specific demethylase 1 (LSD1) catalyzes the removal of mono- and dimethyl modifications of lysine 4 of histone H3 (H3K-4me1/2), which are essential marks of transcriptional activation (*30*). LSD1 has been shown to play a central role in the insurgence of solid and blood cancers (*52*). Specifically, it is highly expressed in AML, a hematopoietic malignancy caused by abnormal proliferation and differentiation of blasts. In AML, LSD1 is crucial for the maintenance of cancer cell stemness, inhibition of cell differentiation, and prevention of apoptosis (*53*). Similar to LSD1, PRMT5, a methyltransferase that catalyzes the SDMA residues, acts as an oncoprotein in AML. PRMT5 activity was shown to support AML growth in vitro and in vivo (*54*, *55*).

Given the involvement of both LSD1 and PRMT5 in AML, the simultaneous inhibition of these enzymes may represent a successful approach to treating this malignancy. Notably, we have identified a synergistic interaction between an LSD1 inhibitor and a PRMT5 inhibitor in multiple AML cell lines. The two inhibitors combined promote AML differentiation, innate immune activation, growth inhibition, and apoptosis.

Our working model is that PRMT5i drives *MDM4 exon 6* skipping, reducing MDM4 protein, and activating p53 transcriptional activity (*36*), whereas LSD1i promotes blast differentiation that can independently enhance p53 accumulation via stress signaling or direct demethylation of P53 (*40*), as reported by multiple groups (*39*, *56*). In combination, PRMT5i's splicing effect on *MDM4* plus LSD1i's increase in p53 protein levels and transcriptional activity (*39*, *40*) jointly elevate the p53 transcriptional output. Alternative models to explain the observed synergy could also be explained by induction of R-loops, RNA/DNA hybrid structures critical for regulating transcription. As single-agent treatments, PRMT5 and LSD1 both induce R-loop formation (*57*, *58*) and combination treatment could lead to the downstream observed effects.

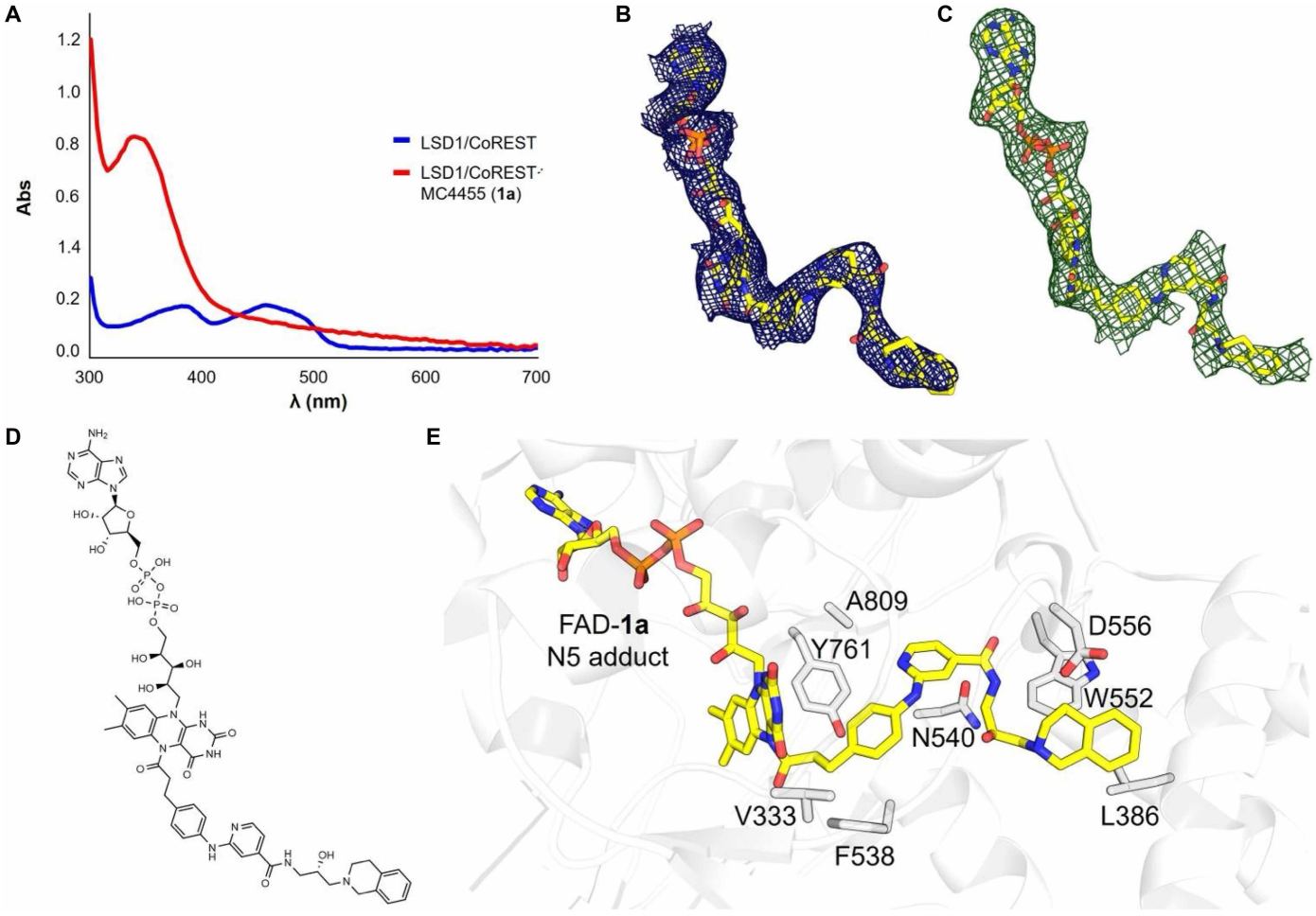

Fig. 6. Structural and spectroscopic characterization of dual LSD1/PRMT5 inhibitor MC4455 (1a). (**A**) Ultraviolet (UV)/visible spectrum of LSD1/CoREST (20 μM) in the oxidized state (blue line) and after 10-min incubation with 200 μM MC4455 (red line). (**B**) $2F_o$-F_c smoothed map of the FAD-N5 adduct with MC4455 contoured at 1.0 σ. The map was calculated before the inclusion of the ligand in the crystallographic refinement. (**C**) Polder omit map calculated excluding the FAD-N5 adduct with the MC4455 adduct and nearby water molecules, contoured at 5 σ. (**D**) Two-dimensional molecular structure of the FAD-N5 adduct with MC4455. (**E**) Binding of MC4455 to the LSD1 active site. The carbon atoms of the FAD and the inhibitor are in yellow, whereas the carbons of the side chains are in gray.

To leverage this synthetic lethal interaction, we developed a series of dual-targeting LSD1/PRMT5 inhibitors that could inhibit both enzymes in vitro in the submicromolar to nanomolar range while being selective over closely related methyltransferases. Among the prepared compounds, two of them impaired leukemic cell viability with higher potency compared to single-target inhibitors and induced apoptosis and myeloid differentiation. In addition, we were able to solve the x-ray cocrystal structure of one of the designed inhibitors with LSD1, thus elucidating its binding mode and providing a structural basis for the rational design of further inhibitors. Although the dual compound had excellent specificity in vitro, further optimization of the molecule is required to enhance solubility and in vivo efficacy. Of note, AML differentiation analysis demonstrated that GSK591 is less potent in inducing differentiation compared to PRT220, pointing at future development of dual inhibitors using PRT220 as a scaffold as a more promising approach.

The concept of dual-targeting molecules holds considerable promise in improving therapeutic efficacy. By targeting two or more molecular pathways simultaneously, these compounds can reduce side effects and enhance patience compliance due to the simplicity of single-drug regimens. In addition to recapitulating the synergy of the two-drug combination, dual inhibitors provide intrinsic advantages, including unified pharmacokinetics, reduced risk of drug-drug interactions, simplified dosing, and improved clinical translatability. This ensures that both inhibitory moieties are simultaneously present within the same cellular environment and, at the same concentration, a feature not guaranteed by loose combinations (*59*–*61*). Previous successes with this approach in the field of epigenetics include the first-in-class dual LSD1/histone deacetylase (HDAC) inhibitor Corin (*47*) and the clinical-stage dual LSD1/HDAC inhibitor JBI-802 (NCT05268666).

MATERIALS AND METHODS

Chemical screen

Cell lines were seeded into 384-well plates with a density of 900 cells per well. Cells were treated at different concentrations of the selected drugs for 7 days (concentrations listed in table S1). Cell viability was measured with the MTS assay (Promega) and normalized to DMSO controls.

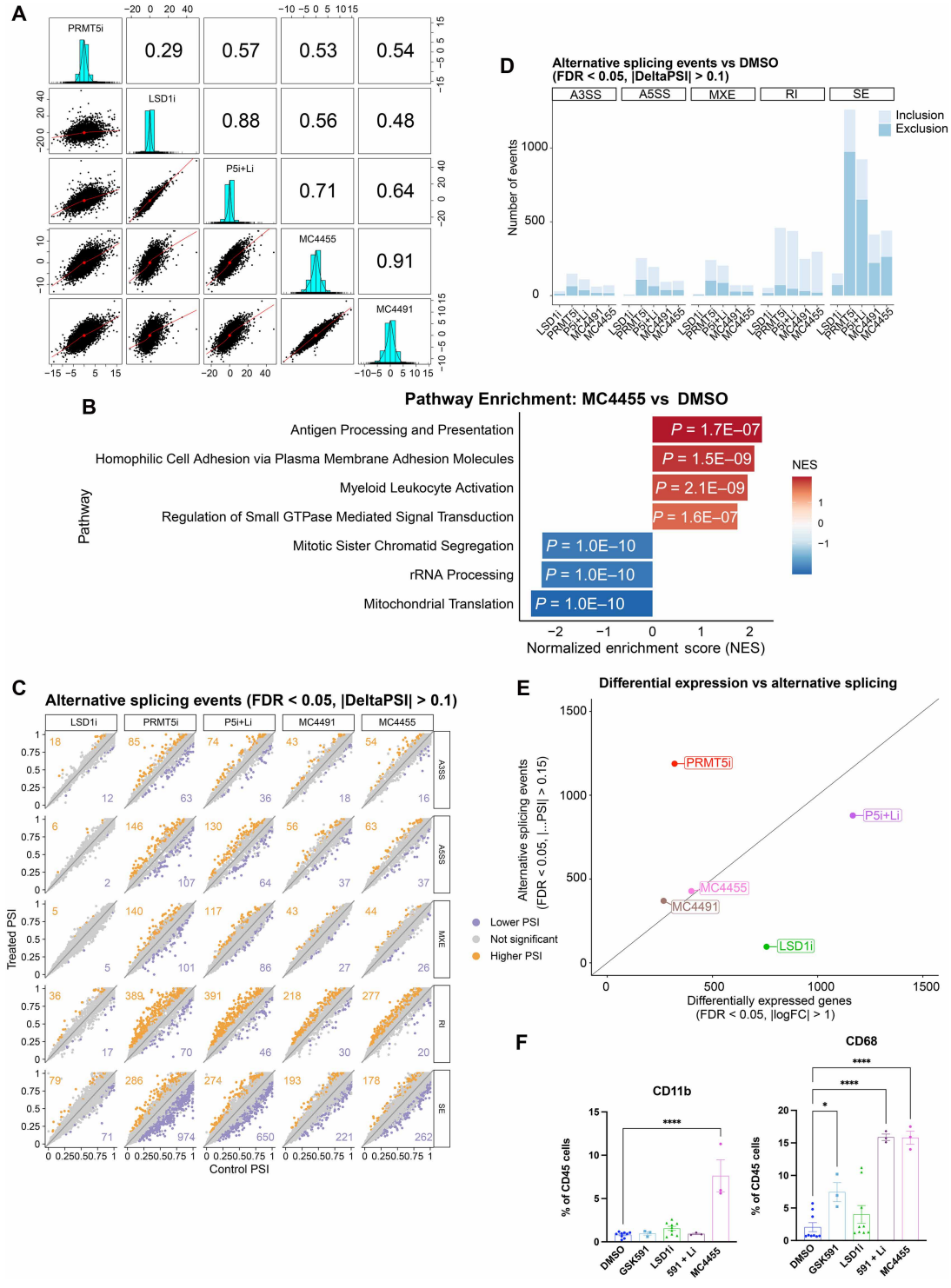

Fig. 7. The dual LSD1/PRMT5 inhibitor recapitulates the effect of drug combination. (**A**) Correlational graphs of differentially expressed genes between PRMT5i, LSD1i, P5i + Li, MC4455, and MC4491 treatment. (**B**) GSEA of MV4-11 cells treated with MC4455 compared to DMSO. (**C**) Differentially expressed alternative splicing events in MV4-11 treated with LSD1i, PRMT5i, P5i + Li, MC4491, and MC4455. ΔPSI levels of each treatment is compared to DMSO. ΔPSI of splicing events > 0.1 is considered significant. Comparison of significant differential gene expression and alternative splicing events in all treatments. (**D**) Alternative splicing events in MV-411 cells treated LSD1i, PRMT5i, P5i + Li, MC4491, or MC4455 for 3 days depicting the following splicing events: A3SS, A5SS, MXE, RI, and SE with inclusion and exclusion. (**E**) Significantly differentially expressed genes versus alternatively spliced genes in all five treatments. FC, fold change. (**F**) Percentage of CD11b- and CD68-expressing cells in CD45 positive in MV4-11 cells treated with DMSO, GSK591, LSD1i, 591 + Li, and MC4455 for 6 days. Statistical analysis performed with one-way ANOVA. Error bars represent SEM. *$P \leq 0.05$; **$P \leq 0.01$; ***$P \leq 0.001$; ****$P \leq 0.0001$.

Human cells lines were maintained in RPMI with 10% phosphate-buffered saline (PBS). Cell viability was measured with CellTiter-Glo (Promega) at either 3 or 7 days of treatment. Fold change apoptosis was measured with Caspase-Glo 3/7 (Promega).

Western blot

Cells were lysed in BC300 buffer [20 mM Tris (pH 7.4), 300 mM KCl, 0.2 mM EDTA, 20% glycerol, 0.1% NP-40, and 10 mM β-mercaptoethanol] and sonicated, and the supernatant was resuspended with Laemmli buffer. Protein concentrations quantified using the RC DC protein assay kit (Bio-Rad). Protein samples were run on 10 or 15% gels and separated by SDS–polyacrylamide gel electrophoresis (PAGE). Transferred samples on to polyvinylidene difluoride (PVDF) membranes and blocked with 5% milk in TBST buffer [0.1% Tween 20 in 1x tris-buffered saline (TBS)] for 1 hour. Membranes were incubated with indicated antibodies and diluted with TBST buffer overnight at 4°C and incubated for 1 hour at room temperature with secondary antibodies. Western blot results were visualized using the SuperSignal West Pico Substrate (Thermo Fisher Scientific 34080) and ChemiDoc (Bio-Rad).

The following antibodies were used: actin (Santa Cruz, SC-47778) at 1:1000, PRMT5 (Abcam, ab109451) at 1:1000, SDMA (Cell Signaling, 13222) at 1:1000, histone 3 (H3) (Abcam, ab1791) at 1:3000, histone H3 (monomethyl K4) (Abcam, ab8895) at 1:1000, histone H3 (dimethyl K4) (Abcam, ab32356) at 1:1000, TP53 (Cell Signaling, 2524) at 1:1000, and MDM4 (Abcam, ab313614) at 1:1000. Band quantification was performed using ImageJ/Fiji software.

Combination index

The CI of Chou-Talalay was used to determine the synergism (*28*)

$$\mathrm{CI} = \frac{(\mathrm{D})_1}{(\mathrm{Dx})_1} + \frac{(\mathrm{D})_2}{(\mathrm{Dx})_1}$$

where $(\mathrm{Dx})_1$ is for $(\mathrm{D})_1$ "alone" that inhibits a system x% and $(\mathrm{Dx})_2$ is for $(\mathrm{D})_2$ "alone" that inhibits a system x%, whereas, in the numerator, $(\mathrm{D})_1 + (\mathrm{D})_2$ is for "in combination" that inhibits x%. The CI value quantitatively defines synergism (CI < 1), additive effect (CI = 1), and antagonism (CI > 1).

Other synergy scores were quantified using the SynergyFinder v3.7.3 R package (*29*). For each drug pair, synergy scores were calculated using four reference models. For HSA, synergy equals the observed effect minus the highest single-agent effect: HSA synergy = observed effect − max(effect of drug A, effect of drug B). For Bliss, the expected effect is Bliss expected = effect A + effect B − (effect A × effect B), and the Bliss synergy score is Bliss synergy = observed effect − Bliss expected. For Loewe, the expected effect is obtained by solving the equation: (dose of A/dose of A that gives the same effect alone) + (dose of B/dose of B that gives the same effect alone) = 1. For ZIP, synergy is the difference between the observed response and the noninteraction surface obtained by jointly fitting the two single-agent dose-response curves.

Flow cytometry

Cells were harvested 6 days posttreatment and incubated in the following antibodies: CD45 (BioLegend, 305019), CD11b (BioLegend, 301333), CD86 (BioLegend, 305427), HLA-DR (BioLegend, 327023), CD45RA (BioLegend, 304165), CD68 (BioLegend, 333807), CD80 (BioLegend, 305219), CD163 (BioLegend, 333617), and CD206 (BioLegend, 321131). Cells were fixed with warm 4% paraformaldehyde and acquired with Cytek Aurora (Cytek Biosciences).

In vivo experiment

LSD1i was dissolved in saline solution (0.9% NaCl) and administered via intraperitoneal injection once per day; PRMT5i was dissolved in 0.5% sodium carboxymethyl cellulose and 0.5% Tween 80 and administered via the oral gavage route once per day. Animals were treated for 5 days/week. NOD/SCID (nonobese diabetic/severe combined immunodeficient) mice (6 to 10 weeks old) were flank injected with 5,000,000 MV4-11 cells.

RNA-seq sample preparation

RNA samples were extracted using the RNeasy mini kit (Qiagen). A modified TruSeq protocol was used to prepare poly(A)-selected, unstranded Illumina libraries. Briefly, 0.5X AMPure XP beads were added to the sample library to select for fragments less than 400 base pairs (bp) followed by 1x beads to select for fragments more than 100 bp. Fragments were amplified using polymerase chain reaction (PCR) (15 cycles) and separated by gel electrophoresis with 2% agarose gel. The 300-bp DNA fragments isolated and sequenced on Illumina HiSeq 2000 (~100 million 101-bp reads per sample).

Reverse transcription PCR

RNA samples were extracted, and cDNA was synthesized using the cDNA synthesis kit (Thermo Fisher Scientific). The following primers were used for validating splicing of MDM4: MDM4 FWD, TGTGGTGGAGATCTTTTGGG; MDM4 REV, GCAGTGTGGGG ATATCGT.

RNA and splicing analysis

Transcript abundances were estimated using Salmon 1.2.1 (*62*) against a transcriptome index built on Ensembl GRCh38 release 99. Abundances were aggregated and collapsed to the gene level using tximeta 1.6.2 (*63*) in an R 4.0.0 environment. Normalization and differential gene expression analysis were performed using DESeq2 1.28.1 (*64*). Heatmaps of gene expression were generated using in-house scripts with R. To quantify alternative splicing, RNA-seq reads were aligned to the human genome (GRCh38 release 99) using STAR 2.7.3a (*65*) and alternative splicing events were identified using rMATS version 4.0.1 (*38*). Statistically significant splicing events were defined using an inclusion level difference of 10% and false discovery rate (FDR) of 0.05.

Pathway analyses, including both overrepresentation analysis (ORA) and Gene Set Enrichment Analysis (GSEA), were performed using clusterProfiler v4.12.6 (*66*) in R. Genes from the differential expression analysis were ranked by the DESeq2 Wald statistic and tested against the GO:BP library, with results filtered at $P < 0.05$ and Benjamini-Hochberg correction. Genes with significant splicing changes (FDR < 0.05 and $|\Delta\mathrm{PSI}| > 0.1$) from retained intron and skipped exon events, identified using rMATS, were mapped to GO:BP pathways via the msigdbr v7.5.1. Pathways were ranked by the number of associated deregulated genes, and the top 10 were visualized using a custom R script.

Biochemistry and molecular modeling

LSD1/CoREST expression

BL21 RP plus cells were transformed with two vectors: pET15b containing His-TEV-trLSD1 and pCDF DUET1 containing His-TEV-

SUMO-trCoREST1. The transformed cells were incubated on an agar plate [ampicillin (25 mg/ml), streptomycin (100 mg/ml), and chloramphenicol (50 mg/ml)] overnight at 37°C. One colony was picked from the plate and inoculated in a starter LB media overnight at 37°C with all three antibiotics. The starter culture was then inoculated into LB media (dilution 1:50) and growth at 37°C until the optical density at 600 nm (OD_{600}) ~ 0.6. The cultures were then chilled a 4°C for ~20 min and then added with 0.4 mM isopropyl-β-D-thiogalactopyranoside (IPTG) and induced at 18°C overnight. Cells were harvested and dissolved in 50 mM Hepes (pH 8), 300 mM NaCl, and 0.5 mM tris(2-carboxyethyl)phosphine (TCEP) containing a mixture of protease inhibitors. Cells were lysed with sonication and harvested at 56,000*g* for 45 min at 4°C, and the resulting supernatant was incubated with 3 ml of Ni-resin (His-Trap, Cytiva) for 30 min at 4°C. After the incubation, the beads were washed for 30 CV with 50 mM Hepes, 300 mM NaCl, and 20 mM imidazole (pH 8) for 5 column volumes (CV) with the same buffer supplemented with 1 M KCl. The protein was eluted with 50 mM Hepes, 300 mM NaCl, and 300 mM imidazole (pH 8). The eluted protein was incubated with SUMO protease (0.005 mg/ml) and dialyzed against 50 mM Hepes and 300 mM NaCl (pH 8). At the end, the stoichiometric complex was obtained by passing the sample through a Superdex 200 10/300 GL with 25 mM Hepes and 5% glycerol (pH 7.2).

LSD1-CoREST binding and inhibition assays

Binding assay was conducted with thermal shift assay measuring the Intrinsic Tryptophan Fluorescence (Tycho, Nanotemper). LSD1-CoREST (10 μM) was incubated with 100 μM **1a** for 10 min at room temperature in 50 mM Hepes (pH 7.5). Controls are carried out with 5% DMSO. Demethylation activity on the histone peptide is registered using a horseradish peroxidase (HRP)–coupled assay monitoring the conversion of Amplex Red into resorufin. Experiments were performed in 96-well plates (Corning) with a plate reader (CLARIOstar, BMG) using a dimethylated H3K4 peptide containing 21 amino acids (purchased from GenScript) as the substrate in 100-μl volume of 50 mM Hepes (pH 7.5). The peptide purity was >95% as checked by analytical high-pressure liquid chromatography and mass spectrometry. The demethylase activity was estimated under aerobic conditions at room temperature by measuring the release of H_2O_2 produced during the catalytic process of the Amplex UltraRed detection system coupled with HRP. Briefly, 300 nM the LSD1/CoREST complex was incubated at room temperature for 10 min in the presence of a range of concentrations of **1a**, 25 mM Amplex UltraRed (Life Technologies), and HRP (0.01 mg/ml; Sigma-Aldrich) in 50 mM Hepes (pH 7.5). The inhibitor was tested in triplicate at each concentration. After preincubation of the enzyme with the inhibitor, the reaction was initiated by adding the dimethylated H3K4 peptide (10 μM). The conversion of the Amplex UltraRed reagent to resorufin was monitored by fluorescence (excitation at 510 nm and emission at 595 nm). Fluorescence data were transformed into hydrogen peroxide concentration through a standard calibration curve. The maximum demethylase activity of LSD1/CoREST was obtained in the absence of the inhibitor and corrected for background fluorescence in the absence of the substrate (5% DMSO was used as a control). The IC_{50} value was calculated using GraphPad Prism version 5.0.3. Flavin absorbance spectrum changes upon addition of **1a** is monitored by nanospectroscopy (ND-1000, Thermo Fisher Scientific).

PRMT1, PRMT5/MEP50, and PRMT7 inhibition assays

PRMT1, PRMT5/MEP50, and PRMT7 inhibition assays were performed by Reaction Biology Corporation (Malvern, PA, USA) using the HotSpot HMT assay. Briefly, human recombinant PRMT1 (catalog no. HMT-11-119), PRMT5/MEP50 complex (catalog no. HMT-22-148), and PRMT7 (catalog no. HMT-21-382) were used at a concentration of 5, 1, and 60 nM, respectively. The appropriate substrate (5 μM histone H4 for PRMT1, 5 μM histone H2A for PRMT5/MEP50, and 5 μM GST-GAR for PRMT7) was added to the reaction buffer [50 mM Tris-HCl (pH 8.5), 5 mM $MgCl_2$, 50 mM NaCl, 0.01% Brij-35, 1 mM dithiothreitol (DTT), and 1% DMSO]. The MT enzyme was delivered into the substrate solution, and the mixture was mixed gently. Afterward, the tested compounds dissolved in DMSO were delivered into the enzyme/substrate reaction mixture by using Acoustic Technology (Echo 550, LabCyte Inc., Sunnyvale, CA) in the nanoliter range, and 1 μM ^{3}H-SAM was also added into the reaction mixture to initiate the reaction. The reaction mixture was incubated for 1 hour at 30°C, and then it was applied to filter paper for detection. The data were analyzed using Excel and GraphPad Prism software for IC_{50} curve fits, where appropriate.

Crystallography

LSD1-CoREST crystals were obtained at 10 mg protein/ml in 0.1 M ADA [*N*-(2-acetamido)iminodiacetic acid, *N*-(carbamoylmethyl) iminodiacetic acid] pH 6.5 and 1.2 M sodium tartrate using published protocols (*67*) and then soaked for 2 hours at 20°C with 1 mM **1a**. The structure determination was performed as described previously (*67*).The crystallographic statistics are listed in table S2.

Molecular docking

Docking was performed with AutoDock Vina (*68*). Default parameters were used except for the "exhaustiveness" parameter, which was set to 30 to ensure thorough sampling of ligand binding conformations. The crystallographic structure of PRMT5/MEP50 in complex with GSK591 and sinefungin (PDB ID: 5C9Z) was prepared as the receptor by removing nonessential water molecules and heteroatoms, adding polar hydrogens, and assigning Gasteiger charges using AutoDockTools. Ligand structures (GSK591 and MC4455) were energy minimized, and all rotatable bonds were set as flexible during conversion to the PDBQT format. The docking search space was defined as a cubic box centered on the GSK591 binding pocket (centered at $X = 24.0$, $Y = -46.0$, and $Z = -11.0$; size of 20 Å by 20 Å by 20 Å for each axis). For validation, GSK591 was redocked with the above parameters, and the best-ranked binding pose was compared to the crystallographic orientation. MC4455 was then docked with the same protocol. Following docking, the predicted protein-ligand complexes were analyzed by visual inspection in PyMOL and by systematic interaction mapping with LigPlot+ (*69*), allowing assessment of hydrogen bonding, hydrophobic contacts, and aromatic interactions.

Supplementary Materials

The PDF file includes:

Figs. S1 to S9
Synthesis of the Hybrid Compounds
Supplementary Methods
Table S11
Legends for tables S1 to S10

Other Supplementary Material for this manuscript includes the following:

Tables S1 to S10

REFERENCES

1. L. Bullinger, K. Döhner, H. Döhner, Genomics of acute myeloid leukemia diagnosis and pathways. *J. Clin. Oncol.* **35**, 934–946 (2017).
2. A. S. Sperling, C. J. Gibson, B. L. Ebert, The genetics of myelodysplastic syndrome: From clonal haematopoiesis to secondary leukaemia. *Nat. Rev. Cancer* **17**, 5–19 (2017).

3. E. Papaemmanuil, M. Gerstung, L. Bullinger, V. I. Gaidzik, P. Paschka, N. D. Roberts, N. E. Potter, M. Heuser, F. Thol, N. Bolli, G. Gundem, P. Van Loo, I. Martincorena, P. Ganly, L. Mudie, S. McLaren, S. O'Meara, K. Raine, D. R. Jones, J. W. Teague, A. P. Butler, M. F. Greaves, A. Ganser, K. Döhner, R. F. Schlenk, H. Döhner, P. J. Campbell, Genomic classification and prognosis in acute myeloid leukemia. *N. Engl. J. Med.* **374**, 2209–2221 (2016).
4. E. R. Mardis, L. Ding, D. J. Dooling, D. E. Larson, M. D. McLellan, K. Chen, D. C. Koboldt, R. S. Fulton, K. D. Delehaunty, S. D. McGrath, L. A. Fulton, D. P. Locke, V. J. Magrini, R. M. Abbott, T. L. Vickery, J. S. Reed, J. S. Robinson, T. Wylie, S. M. Smith, L. Carmichael, J. M. Eldred, C. C. Harris, J. Walker, J. B. Peck, F. Du, A. F. Dukes, G. E. Sanderson, A. M. Brummett, E. Clark, J. F. McMichael, R. J. Meyer, J. K. Schindler, C. S. Pohl, J. W. Wallis, X. Shi, L. Lin, H. Schmidt, Y. Tang, C. Haipek, M. E. Wiechert, J. V. Ivy, J. Kalicki, G. Elliott, R. E. Ries, J. E. Payton, P. Westervelt, M. H. Tomasson, M. A. Watson, J. Baty, S. Heath, W. D. Shannon, R. Nagarajan, D. C. Link, M. J. Walter, T. A. Graubert, J. F. DiPersio, R. K. Wilson, T. J. Ley, Recurring mutations found by sequencing an acute myeloid leukemia genome. *N. Engl. J. Med.* **361**, 1058–1066 (2009).
5. I. De Kouchkovsky, M. Abdul-Hay, Acute myeloid leukemia: A comprehensive review and 2016 update. *Blood Cancer J.* **6**, e441 (2016).
6. F. Wachter, Y. Pikman, Pathophysiology of acute myeloid leukemia. *Acta Haematol.* **147**, 229–246 (2024).
7. J. Shi, E. Wang, J. P. Milazzo, Z. Wang, J. B. Kinney, C. R. Vakoc, Discovery of cancer drug targets by CRISPR-Cas9 screening of protein domains. *Nat. Biotechnol.* **33**, 661–667 (2015).
8. E. Guccione, S. Richard, The regulation, functions and clinical relevance of arginine methylation. *Nat. Rev. Mol. Cell Biol.* **20**, 642–657 (2019).
9. E. Guccione, M. Schwarz, F. Di Tullio, S. Mzoughi, Cancer synthetic vulnerabilities to protein arginine methyltransferase inhibitors. *Curr. Opin. Pharmacol.* **59**, 33–42 (2021).
10. C. M. Koh, M. Bezzi, D. H. Low, W. X. Ang, S. X. Teo, F. P. Gay, M. Al-Haddawi, S. Y. Tan, M. Osato, A. Sabò, B. Amati, K. B. Wee, E. Guccione, MYC regulates the core pre-mRNA splicing machinery as an essential step in lymphomagenesis. *Nature* **523**, 96–100 (2015).
11. L. C. Litzler, A. Zahn, A. P. Meli, S. Hébert, A. M. Patenaude, S. P. Methot, A. Sprumont, T. Bois, D. Kitamura, S. Costantino, I. L. King, C. L. Kleinman, S. Richard, J. M. Di Noia, PRMT5 is essential for B cell development and germinal center dynamics. *Nat. Commun.* **10**, 22 (2019).
12. G. V. Kryukov, F. H. Wilson, J. R. Ruth, J. Paulk, A. Tsherniak, S. E. Marlow, F. Vazquez, B. A. Weir, M. E. Fitzgerald, M. Tanaka, C. M. Bielski, J. M. Scott, C. Dennis, G. S. Cowley, J. S. Boehm, D. E. Root, T. R. Golub, C. B. Clish, J. E. Bradner, W. C. Hahn, L. A. Garraway, MTAP deletion confers enhanced dependency on the PRMT5 arginine methyltransferase in cancer cells. *Science* **351**, 1214–1218 (2016).
13. K. Marjon, M. J. Cameron, P. Quang, M. F. Clasquin, E. Mandley, K. Kunii, M. McVay, S. Choe, A. Kernytsky, S. Gross, Z. Konteatis, J. Murtie, M. L. Blake, J. Travins, M. Dorsch, S. A. Biller, K. M. Marks, MTAP deletions in cancer create vulnerability to targeting of the MAT2A/PRMT5/RIOK1 axis. *Cell Rep.* **15**, 574–587 (2016).
14. K. J. Mavrakis, E. R. McDonald III, M. R. Schlabach, E. Billy, G. R. Hoffman, A. deWeck, D. A. Ruddy, K. Venkatesan, J. Yu, G. McAllister, M. Stump, R. deBeaumont, S. Ho, Y. Yue, Y. Liu, Y. Yan-Neale, G. Yang, F. Lin, H. Yin, H. Gao, D. R. Kipp, S. Zhao, J. T. McNamara, E. R. Sprague, B. Zheng, Y. Lin, Y. S. Cho, J. Gu, K. Crawford, D. Ciccone, A. C. Vitari, A. Lai, V. Capka, K. Hurov, J. A. Porter, J. Tallarico, C. Mickanin, E. Lees, R. Pagliarini, N. Keen, T. Schmelzle, F. Hofmann, F. Stegmeier, W. R. Sellers, Disordered methionine metabolism in MTAP/CDKN2A-deleted cancers leads to dependence on PRMT5. *Science* **351**, 1208–1213 (2016).
15. A. Fedoriw, S. R. Rajapurkar, S. O'Brien, S. V. Gerhart, L. H. Mitchell, N. D. Adams, N. Rioux, T. Lingaraj, S. A. Ribich, M. B. Pappalardi, N. Shah, J. Laraio, Y. Liu, M. Butticello, C. L. Carpenter, C. Creasy, S. Korenchuk, M. T. McCabe, C. F. McHugh, R. Nagarajan, C. Wagner, F. Zappacosta, R. Annan, N. O. Concha, R. A. Thomas, T. K. Hart, J. J. Smith, R. A. Copeland, M. P. Moyer, J. Campbell, K. Stickland, J. Mills, S. Jacques-O'Hagan, C. Allain, D. Johnston, A. Raimondi, M. Porter Scott, N. Waters, K. Swinger, A. Boriack-Sjodin, T. Riera, G. Shapiro, R. Chesworth, R. K. Prinjha, R. G. Kruger, O. Barbash, H. P. Mohammad, Anti-tumor activity of the type I PRMT inhibitor, GSK3368715, synergizes with PRMT5 inhibition through MTAP loss. *Cancer Cell* **36**, 100–114.e25 (2019).
16. G. Gao, L. Zhang, O. D. Villarreal, W. He, D. Su, E. Bedford, P. Moh, J. Shen, X. Shi, M. T. Bedford, H. Xu, PRMT1 loss sensitizes cells to PRMT5 inhibition. *Nucleic Acids Res.* **47**, 5038–5048 (2019).
17. J. Y. Fong, L. Pignata, P. A. Goy, K. C. Kawabata, S. C. Lee, C. M. Koh, D. Musiani, E. Massignani, A. G. Kotini, A. Penson, C. M. Wun, Y. Shen, M. Schwarz, D. H. Low, A. Rialdi, M. Ki, H. Wollmann, S. Mzoughi, F. Gay, C. Thompson, T. Hart, O. Barbash, G. M. Luciani, M. M. Szewczyk, B. J. Wouters, R. Delwel, E. P. Papapetrou, D. Barsyte-Lovejoy, C. H. Arrowsmith, M. D. Minden, J. Jin, A. Melnick, T. Bonaldi, O. Abdel-Wahab, E. Guccione, Therapeutic targeting of RNA splicing catalysis through inhibition of protein arginine methylation. *Cancer Cell* **36**, 194–209.e9 (2019).
18. M. Yang, C. B. Gocke, X. Luo, D. Borek, D. R. Tomchick, M. Machius, Z. Otwinowski, H. Yu, Structural basis for CoREST-dependent demethylation of nucleosomes by the human LSD1 histone demethylase. *Mol. Cell* **23**, 377–387 (2006).
19. M. G. Lee, C. Wynder, N. Cooch, R. Shiekhattar, An essential role for CoREST in nucleosomal histone 3 lysine 4 demethylation. *Nature* **437**, 432–435 (2005).
20. J. Wang, S. Hevi, J. K. Kurash, H. Lei, F. Gay, J. Bajko, H. Su, W. Sun, H. Chang, G. Xu, F. Gaudet, E. Li, T. Chen, The lysine demethylase LSD1 (KDM1) is required for maintenance of global DNA methylation. *Nat. Genet.* **41**, 125–129 (2009).
21. B. Perillo, M. N. Ombra, A. Bertoni, C. Cuozzo, S. Sacchetti, A. Sasso, L. Chiariotti, A. Malorni, C. Abbondanza, E. V. Avvedimento, DNA oxidation as triggered by H3K9me2 demethylation drives estrogen-induced gene expression. *Science* **319**, 202–206 (2008).
22. E. Metzger, M. Wissmann, N. Yin, J. M. Müller, R. Schneider, A. H. Peters, T. Günther, R. Buettner, R. Schüle, LSD1 demethylates repressive histone marks to promote androgen-receptor-dependent transcription. *Nature* **437**, 436–439 (2005).
23. M. Wissmann, N. Yin, J. M. Müller, H. Greschik, B. D. Fodor, T. Jenuwein, C. Vogler, R. Schneider, T. Günther, R. Buettner, E. Metzger, R. Schüle, Cooperative demethylation by JMJD2C and LSD1 promotes androgen receptor-dependent gene expression. *Nat. Cell Biol.* **9**, 347–353 (2007).
24. I. Garcia-Bassets, Y. S. Kwon, F. Telese, G. G. Prefontaine, K. R. Hutt, C. S. Cheng, B. G. Ju, K. A. Ohgi, J. Wang, L. Escoubet-Lozach, D. W. Rose, C. K. Glass, X. D. Fu, M. G. Rosenfeld, Histone methylation-dependent mechanisms impose ligand dependency for gene activation by nuclear receptors. *Cell* **128**, 505–518 (2007).
25. D. Barsyte-Lovejoy, M. M. Szewczyk, P. Prinos, E. Lima-Fernandes, S. Ackloo, C. H. Arrowsmith, Chemical biology approaches for characterization of epigenetic regulators. *Methods Enzymol.* **574**, 79–103 (2016).
26. X. Wei, J. Yang, S. J. Adair, H. Ozturk, C. Kuscu, K. Y. Lee, W. J. Kane, P. E. O'Hara, D. Liu, Y. M. Demirlenk, A. H. Habieb, E. Yilmaz, A. Dutta, T. W. Bauer, M. Adli, Targeted CRISPR screening identifies PRMT5 as synthetic lethality combinatorial target with gemcitabine in pancreatic cancer cells. *Proc. Natl. Acad. Sci. U.S.A.* **117**, 28068–28079 (2020).
27. K. Bajbouj, R. K. Ramakrishnan, M. Saber-Ayad, H. A. Omar, N. Saheb Sharif-Askari, J. Shafarin, A. B. Elmoselhi, A. Ihmaid, S. AlHaj Ali, A. Alalool, R. Abdullah, Q. Hamid, PRMT5 selective inhibitor enhances therapeutic efficacy of cisplatin in lung cancer cells. *Int. J. Mol. Sci.* **22**, 6131 (2021).
28. T. C. Chou, Drug combination studies and their synergy quantification using the Chou-Talalay method. *Cancer Res.* **70**, 440–446 (2010).
29. S. Zheng, W. Wang, J. Aldahdooh, A. Malyutina, T. Shadbahr, Z. Tanoli, A. Pessia, J. Tang, SynergyFinder Plus: Toward better interpretation and annotation of drug combination screening datasets. *Genomics Proteomics Bioinformatics* **20**, 587–596 (2022).
30. D. Rotili, A. Mai, Targeting histone demethylases: A new avenue for the fight against cancer. *Genes Cancer* **2**, 663–679 (2011).
31. D. Musiani, J. Bok, E. Massignani, L. Wu, T. Tabaglio, M. R. Ippolito, A. Cuomo, U. Ozbek, H. Zorgati, U. Ghoshdastider, R. C. Robinson, E. Guccione, T. Bonaldi, Proteomics profiling of arginine methylation defines PRMT5 substrate specificity. *Sci. Signal.* **12**, eaat8388 (2019).
32. W. J. Friesen, S. Paushkin, A. Wyce, S. Massenet, G. S. Pesiridis, G. Van Duyne, J. Rappsilber, M. Mann, G. Dreyfuss, The methylosome, a 20S complex containing JBP1 and pICln, produces dimethylarginine-modified Sm proteins. *Mol. Cell. Biol.* **21**, 8289–8300 (2001).
33. G. Meister, C. Eggert, D. Bühler, H. Brahms, C. Kambach, U. Fischer, Methylation of Sm proteins by a complex containing PRMT5 and the putative U snRNP assembly factor pICln. *Curr. Biol.* **11**, 1990–1994 (2001).
34. G. Meister, U. Fischer, Assisted RNP assembly: SMN and PRMT5 complexes cooperate in the formation of spliceosomal UsnRNPs. *EMBO J.* **21**, 5853–5863 (2002).
35. M. Dewaele, T. Tabaglio, K. Willekens, M. Bezzi, S. X. Teo, D. H. Low, C. M. Koh, F. Rambow, M. Fiers, A. Rogiers, E. Radaelli, M. Al-Haddawi, S. Y. Tan, E. Hermans, F. Amant, H. Yan, M. Lakshmanan, R. C. Koumar, S. T. Lim, F. A. Derheimer, R. M. Campbell, Z. Bonday, V. Tergaonkar, M. Shackleton, C. Blattner, J. C. Marine, E. Guccione, Antisense oligonucleotide-mediated MDM4 exon 6 skipping impairs tumor growth. *J. Clin. Invest.* **126**, 68–84 (2016).
36. M. Bezzi, S. X. Teo, J. Muller, W. C. Mok, S. K. Sahu, L. A. Vardy, Z. Q. Bonday, E. Guccione, Regulation of constitutive and alternative splicing by PRMT5 reveals a role for Mdm4 pre-mRNA in sensing defects in the spliceosomal machinery. *Genes Dev.* **27**, 1903–1916 (2013).
37. P. J. Hamard, G. E. Santiago, F. Liu, D. L. Karl, C. Martinez, N. Man, A. K. Mookhtiar, S. Duffort, S. Greenblatt, R. E. Verdun, S. D. Nimer, PRMT5 regulates DNA repair by controlling the alternative splicing of histone-modifying enzymes. *Cell Rep.* **24**, 2643–2657 (2018).
38. S. Shen, J. W. Park, Z. X. Lu, L. Lin, M. D. Henry, Y. N. Wu, Q. Zhou, Y. Xing, rMATS: Robust and flexible detection of differential alternative splicing from replicate RNA-Seq data. *Proc. Natl. Acad. Sci. U.S.A.* **111**, E5593–E5601 (2014).
39. S. F. Cai, S. H. Chu, A. D. Goldberg, S. Parvin, R. P. Koche, J. L. Glass, E. M. Stein, M. S. Tallman, F. Sen, C. A. Famulare, M. Cusan, C. H. Huang, C. W. Chen, L. Zou, K. B. Cordner, N. L. DelGaudio, V. Durani, M. Kini, M. Rex, H. S. Tian, J. Zuber, T. Baslan, S. W. Lowe, H. Y. Rienhoff Jr., A. Letai, R. L. Levine, S. A. Armstrong, Leukemia cell of origin influences apoptotic priming and sensitivity to LSD1 inhibition. *Cancer Discov.* **10**, 1500–1513 (2020).

40. J. Huang, R. Sengupta, A. B. Espejo, M. G. Lee, J. A. Dorsey, M. Richter, S. Opravil, R. Shiekhattar, M. T. Bedford, T. Jenuwein, S. L. Berger, p53 is regulated by the lysine demethylase LSD1. *Nature* **449**, 105–108 (2007).
41. D. Rotili, S. Tomassi, M. Conte, R. Benedetti, M. Tortorici, G. Ciossani, S. Valente, B. Marrocco, D. Labella, E. Novellino, A. Mattevi, L. Altucci, A. Tumber, C. Yapp, O. N. King, R. J. Hopkinson, A. Kawamura, C. J. Schofield, A. Mai, Pan-histone demethylase inhibitors simultaneously targeting Jumonji C and lysine-specific demethylases display high anticancer activities. *J. Med. Chem.* **57**, 42–55 (2014).
42. P. Vianello, O. A. Botrugno, A. Cappa, G. Ciossani, P. Dessanti, A. Mai, A. Mattevi, G. Meroni, S. Minucci, F. Thaler, M. Tortorici, P. Trifiró, S. Valente, M. Villa, M. Varasi, C. Mercurio, Synthesis, biological activity and mechanistic insights of 1-substituted cyclopropylamine derivatives: A novel class of irreversible inhibitors of histone demethylase KDM1A. *Eur. J. Med. Chem.* **86**, 352–363 (2014).
43. S. Valente, V. Rodriguez, C. Mercurio, P. Vianello, B. Saponara, R. Cirilli, G. Ciossani, D. Labella, B. Marrocco, D. Monaldi, G. Ruoppolo, M. Tilset, O. A. Botrugno, P. Dessanti, S. Minucci, A. Mattevi, M. Varasi, A. Mai, Pure enantiomers of benzoylamino-tranylcypromine: LSD1 inhibition, gene modulation in human leukemia cells and effects on clonogenic potential of murine promyelocytic blasts. *Eur. J. Med. Chem.* **94**, 163–174 (2015).
44. S. Valente, V. Rodriguez, C. Mercurio, P. Vianello, B. Saponara, R. Cirilli, G. Ciossani, D. Labella, B. Marrocco, G. Ruoppolo, O. A. Botrugno, P. Dessanti, S. Minucci, A. Mattevi, M. Varasi, A. Mai, Pure diastereomers of a tranylcypromine-based LSD1 inhibitor: Enzyme selectivity and in-cell studies. *ACS Med. Chem. Lett.* **6**, 173–177 (2015).
45. V. Rodriguez, S. Valente, S. Rovida, D. Rotili, G. Stazi, A. Lucidi, G. Ciossani, A. Mattevi, O. A. Botrugno, P. Dessanti, C. Mercurio, P. Vianello, S. Minucci, M. Varasi, A. Mai, Pyrrole- and indole-containing tranylcypromine derivatives as novel lysine-specific demethylase 1 inhibitors active on cancer cells. *MedChemComm* **6**, 665–670 (2015).
46. P. Vianello, O. A. Botrugno, A. Cappa, R. Dal Zuffo, P. Dessanti, A. Mai, B. Marrocco, A. Mattevi, G. Meroni, S. Minucci, G. Stazi, F. Thaler, P. Trifiró, S. Valente, M. Villa, M. Varasi, C. Mercurio, Discovery of a novel inhibitor of histone lysine-specific demethylase 1A (KDM1A/LSD1) as orally active antitumor agent. *J. Med. Chem.* **59**, 1501–1517 (2016).
47. J. H. Kalin, M. Wu, A. V. Gomez, Y. Song, J. Das, D. Hayward, N. Adejola, M. Wu, I. Panova, H. J. Chung, E. Kim, H. J. Roberts, J. M. Roberts, P. Prusevich, J. R. Jeliazkov, S. S. Roy Burman, L. Fairall, C. Milano, A. Eroglu, C. M. Proby, A. T. Dinkova-Kostova, W. W. Hancock, J. J. Gray, J. E. Bradner, S. Valente, A. Mai, N. M. Anders, M. A. Rudek, Y. Hu, B. Ryu, J. W. R. Schwabe, A. Mattevi, R. M. Alani, P. A. Cole, Targeting the CoREST complex with dual histone deacetylase and demethylase inhibitors. *Nat. Commun.* **9**, 53 (2018).
48. R. Fioravanti, A. Romanelli, N. Mautone, E. Di Bello, A. Rovere, D. Corinti, C. Zwergel, S. Valente, D. Rotili, O. A. Botrugno, P. Dessanti, S. Vultaggio, P. Vianello, A. Cappa, C. Binda, A. Mattevi, S. Minucci, C. Mercurio, M. Varasi, A. Mai, Tranylcypromine-based LSD1 inhibitors: Structure-activity relationships, antiproliferative effects in leukemia, and gene target modulation. *ChemMedChem* **15**, 643–658 (2020).
49. R. Fioravanti, V. Rodriguez, J. Caroli, U. Chianese, R. Benedetti, E. D. Bello, B. Noce, C. Zwergel, D. Corinti, D. Viña, L. Altucci, A. Mattevi, S. Valente, A. Mai, Heterocycle-containing tranylcypromine derivatives endowed with high anti-LSD1 activity. *J. Enzyme Inhib. Med. Chem.* **37**, 973–985 (2022).
50. K. W. Duncan, N. Rioux, P. A. Boriack-Sjodin, M. J. Munchhof, L. A. Reiter, C. R. Majer, L. Jin, L. D. Johnston, E. Chan-Penebre, K. G. Kuplast, M. Porter Scott, R. M. Pollock, N. J. Waters, J. J. Smith, M. P. Moyer, R. A. Copeland, R. Chesworth, Structure and property guided design in the identification of PRMT5 tool compound EPZ015666. *ACS Med. Chem. Lett.* **7**, 162–166 (2016).
51. C. Binda, S. Valente, M. Romanenghi, S. Pilotto, R. Cirilli, A. Karytinos, G. Ciossani, O. A. Botrugno, F. Forneris, M. Tardugno, D. E. Edmondson, S. Minucci, A. Mattevi, A. Mai, Biochemical, structural, and biological evaluation of tranylcypromine derivatives as inhibitors of histone demethylases LSD1 and LSD2. *J. Am. Chem. Soc.* **132**, 6827–6833 (2010).
52. B. Noce, E. Di Bello, R. Fioravanti, A. Mai, LSD1 inhibitors for cancer treatment: Focus on multi-target agents and compounds in clinical trials. *Front. Pharmacol.* **14**, 1120911 (2023).
53. R. Ravasio, E. Ceccacci, L. Nicosia, A. Hosseini, P. L. Rossi, I. Barozzi, L. Fornasari, R. D. Zuffo, S. Valente, R. Fioravanti, C. Mercurio, M. Varasi, A. Mattevi, A. Mai, G. Pavesi, T. Bonaldi, S. Minucci, Targeting the scaffolding role of LSD1 (KDM1A) poises acute myeloid leukemia cells for retinoic acid-induced differentiation. *Sci. Adv.* **6**, eaax2746 (2020).
54. A. Radzisheuskaya, P. V. Shliaha, V. Grinev, E. Lorenzini, S. Kovalchuk, D. Shlyueva, V. Gorshkov, R. C. Hendrickson, O. N. Jensen, K. Helin, PRMT5 methylome profiling uncovers a direct link to splicing regulation in acute myeloid leukemia. *Nat. Struct. Mol. Biol.* **26**, 999–1012 (2019).
55. S. S. Tarighat, R. Santhanam, D. Frankhouser, H. S. Radomska, H. Lai, M. Anghelina, H. Wang, X. Huang, L. Alinari, A. Walker, M. A. Caligiuri, C. M. Croce, L. Li, R. Garzon, C. Li, R. A. Baiocchi, G. Marcucci, The dual epigenetic role of PRMT5 in acute myeloid leukemia: Gene activation and repression via histone arginine methylation. *Leukemia* **30**, 789–799 (2016).
56. S. Gupta, K. Doyle, T. L. Mosbruger, A. Butterfield, A. Weston, A. Ast, M. Kaadige, A. Verma, S. Sharma, Reversible LSD1 inhibition with HCI-2509 induces the p53 gene expression signature and disrupts the MYCN signature in high-risk neuroblastoma cells. *Oncotarget* **9**, 9907–9924 (2018).
57. S. Pinter, F. Knodel, M. Choudalakis, P. Schnee, C. Kroll, M. Fuchs, A. Broehm, S. Weirich, M. Roth, S. A. Eisler, J. Zuber, A. Jeltsch, P. Rathert, A functional LSD1 coregulator screen reveals a novel transcriptional regulatory cascade connecting R-loop homeostasis with epigenetic regulation. *Nucleic Acids Res.* **49**, 4350–4370 (2021).
58. P. Kalev, M. L. Hyer, S. Gross, Z. Konteatis, C. C. Chen, M. Fletcher, M. Lein, E. Aguado-Fraile, V. Frank, A. Barnett, E. Mandley, J. Goldford, Y. Chen, K. Sellers, S. Hayes, K. Lizotte, P. Quang, Y. Tuncay, M. Clasquin, R. Peters, J. Weier, E. Simone, J. Murtie, W. Liu, R. Nagaraja, L. Dang, Z. Sui, S. A. Biller, J. Travins, K. M. Marks, K. Marjon, MAT2A inhibition blocks the growth of MTAP-deleted cancer cells by reducing PRMT5-dependent mRNA splicing and inducing DNA damage. *Cancer Cell* **39**, 209–224.e11 (2021).
59. D. Tomaselli, A. Lucidi, D. Rotili, A. Mai, Epigenetic polypharmacology: A new frontier for epi-drug discovery. *Med. Res. Rev.* **40**, 190–244 (2020).
60. A. Anighoro, J. Bajorath, G. Rastelli, Polypharmacology: Challenges and opportunities in drug discovery. *J. Med. Chem.* **57**, 7874–7887 (2014).
61. G. Stazi, R. Fioravanti, A. Mai, A. Mattevi, S. Valente, Histone deacetylases as an epigenetic pillar for the development of hybrid inhibitors in cancer. *Curr. Opin. Chem. Biol.* **50**, 89–100 (2019).
62. R. Patro, G. Duggal, M. I. Love, R. A. Irizarry, C. Kingsford, Salmon provides fast and bias-aware quantification of transcript expression. *Nat. Methods* **14**, 417–419 (2017).
63. M. I. Love, C. Soneson, P. F. Hickey, L. K. Johnson, N. T. Pierce, L. Shepherd, M. Morgan, R. Patro, Tximeta: Reference sequence checksums for provenance identification in RNA-seq. *PLOS Comput. Biol.* **16**, e1007664 (2020).
64. M. I. Love, W. Huber, S. Anders, Moderated estimation of fold change and dispersion for RNA-seq data with DESeq2. *Genome Biol.* **15**, 550 (2014).
65. A. Dobin, C. A. Davis, F. Schlesinger, J. Drenkow, C. Zaleski, S. Jha, P. Batut, M. Chaisson, T. R. Gingeras, STAR: Ultrafast universal RNA-seq aligner. *Bioinformatics* **29**, 15–21 (2013).
66. T. Wu, E. Hu, S. Xu, M. Chen, P. Guo, Z. Dai, T. Feng, L. Zhou, W. Tang, L. Zhan, X. Fu, S. Liu, X. Bo, G. Yu, clusterProfiler 4.0: A universal enrichment tool for interpreting omics data. *Innovation* **2**, 100141 (2021).
67. F. Forneris, C. Binda, A. Dall'Aglio, M. W. Fraaije, E. Battaglioli, A. Mattevi, A highly specific mechanism of histone H3-K4 recognition by histone demethylase LSD1. *J. Biol. Chem.* **281**, 35289–35295 (2006).
68. J. Eberhardt, D. Santos-Martins, A. F. Tillack, S. Forli, AutoDock Vina 1.2.0: New docking methods, expanded force field, and python bindings. *J. Chem. Inf. Model.* **61**, 3891–3898 (2021).
69. R. A. Laskowski, M. B. Swindells, LigPlot+: Multiple ligand-protein interaction diagrams for drug discovery. *J. Chem. Inf. Model.* **51**, 2778–2786 (2011).

Acknowledgments: We acknowledge O. Abdel-Wahab for reagents and fruitful discussions. We gratefully acknowledge use of the services and facilities of the Tisch Cancer Institute supported by the NCI Cancer Center Support Grant (P30 CA196521). This work was supported in part by the Bioinformatics for Next Generation Sequencing (BiNGS) shared resource facility within the Tisch Cancer Institute at the Icahn School of Medicine at Mount Sinai, which is partially supported by NIH grant P30CA196521. This work was also supported in part through the computational resources and staff expertise provided by Scientific Computing at the Icahn School of Medicine at Mount Sinai and supported by the Clinical and Translational Science Awards (CTSA) grant UL1TR004419 from the National Center for Advancing Translational Sciences. We are grateful to the members of the Dean's Flow Cytometry CORE at Mount Sinai. **Funding:** Research reported in this publication was supported by the ISMMS seed fund to E.G. and the National Cancer Institute (NCI) of the National Institutes of Health grant RO1CA249204 to E.G. This work was supported by the MSCA Postdoctoral Fellowship 2021 (101062363, EpiPolyPharma) to F.F., Associazione Italiana per la Ricerca sul Cancro (IG26172) and Ateneo Sapienza Project 2020 (RG120172B8E53D03) to S.V., PRIN2022 (P2022FESRR to A. Mai), and Associazione Italiana per la Ricerca sul Cancro (IG31139 to A. Mai). **Author contributions:** Overall design of the project, conceptualization, and writing: N.J.P., E.A., L.P., F.F., S.V., A. Mai, and E.G. Acquisition of experimental data and investigation: N.J.P., L.P., F.F., E.A., J.Y.F., Y.H., C.L., E.D.B., C.C., M.B., M.S., C.A., S.N., T.T., A.D.J., M.L., R.C., and T.M. Detailed molecular and genomics approaches: L.P., E.A., T.M., T.B., and E.G. Generation of reagents and scientific inputs: F.F., E.D.B., C.C., M.B., K.I., P.S., A.D.J., A. Mattevi, S.V., D.K.B.W., and A. Mai. Bioinformatic analysis: D.T., P.-A.G., and N.G.-T. Resources: P.S. and C.A. Funding acquisition: A. Mai and E.G. Organization of experiments and figures: N.J.P., L.P., F.F., E.A., T.B., S.V., A. Mattevi, and E.G. N.J.P., E.A., F.F., L.P., S.V., A. Mai, and E.G. wrote the manuscript with comments from all authors. **Competing interests:** The Guccione laboratory received research funds from Prelude Therapeutics. E.G. is a cofounder, shareholder, consultant, and advisory board member of Prometeo Therapeutics. The other authors declare that they have no competing interests. **Data, code, and materials availability:** All data and code needed to evaluate and reproduce the results in the paper are present in the paper and/or the Supplementary Materials. All transcriptome (RNA-seq) data supporting the findings of this study have been deposited in the NCBI Gene Expression

Omnibus under accession number GSE278623. Chemical and biochemical data relative to this study have been deposited to figshare (https://doi.org/10.6084/m9.figshare.30940520). New physical materials generated from this study are described in the Materials and Methods and Supplementary Materials.

Submitted 8 July 2025
Accepted 25 February 2026
Published 27 March 2026
10.1126/sciadv.aea4059

ScienceAdvances

A synergistic interaction between PRMT5 and LSD1 inhibitors in AML

Nesteene Joy Param, Elisa Arceci, Francesco Fiorentino, Luca Pignata, Denis Torre, Nayeli Gutiérrez-Trejo, Jia Yi Fong, Pierre-Alexis Goy, Brenda Y. Han, Chiara Lambona, Elisabetta Di Bello, Carola Castiello, Marco Barone, Megan Schwarz, Cheryl Arrowsmith, Koichi Ito, Peggy Scherle, Dave Keng Boon Wee, Steven Ndoye, Tommaso Tabaglio, Anand D. Jeyasekharan, Manikandan Lakshmanan, Roberto Cirilli, Hansjörg Habisch, Tobias Madl, Andrea Mattevi, Sergio Valente, Antonello Mai, and Ernesto Guccione

Sci. Adv. **12** (13), eaea4059. DOI: 10.1126/sciadv.aea4059

Science Advances (ISSN 2375-2548) is published by the American Association for the Advancement of Science. 1200 New York Avenue NW, Washington, DC 20005. The title *Science Advances* is a registered trademark of AAAS.